NCAR/TN-130+STR
NCAR TECHNICAL NOTE

September 1978

Case Studies on Convective Storms
Case Study 1

22 June 1976: First Echo Case

Daniel W. Breed

CONVECTIVE STORMS DIVISION

NATIONAL CENTER FOR ATMOSPHERIC RESEARCH
BOULDER, COLORADO

FOREWORD

This is one of a series of Technical Notes reporting data on aircraft penetrations in convective clouds, ranging from cumulus congestus to thunderstorms, in northeastern Colorado and adjacent portions of Wyoming and Nebraska. The June and July 1976 field season of the National Hail Research Experiment is the setting of the first six to ten of these Notes. The series may be extended later to the 1974, 1975 and 1978 seasons. All of the cases involve aircraft data, including vertical velocity, state parameters and cloud physical data, obtained in coordination with detailed S-band radar scans, normally taken with about two minute time resolution.

Some of these cases will be the subject matter of formal publications, in which case the Tech Note will supplement the publication by providing a more extensive presentation of data. Other cases will be presented as complete sets of data only in the Tech Notes, but usually some portions of the data will be included in publications on general properties of convective clouds over the high plains.

These Tech Notes will always have the following components: a brief synoptic setting, a representative sounding, a brief, general radar reflectivity history, a more detailed radar history of the cloud or storm investigated with the aircraft tracks superimposed, a presentation of the aircraft data, and a discussion. The presentation will not be truly complete either as regards radar data or cloud droplet or precipitation particle size spectra, because these data are too voluminous. However, the general data, such as particle concentrations and

liquid water content, will be presented along with some examples of the more complete data and remarks on typical aspects.

The data quality is in some cases difficult to assess. There is no absolute standard for many in-cloud measurements, even of temperature. Trust in the listed values for liquid water content and droplet sizes and concentrations must always be qualified to some degree. These Technical Notes will include remarks on data quality that record the opinions of those closest to taking the data, and the reasons for the opinions. Work on the data reliability will be continuing, however, and because of this, some of these opinions may change. Any such changes will be recorded in the Tech Note series, along with reference to previous notes in which changes should be made.

The penetrating aircraft for the 1976 season were the NCAR/NOAA sailplane, the University of Wyoming Queen Air, and the South Dakota School of Mines and Technology armored T-28.

This series of Tech Notes is intended to provide a lasting record of cloud data in the high plains area that may be of use in unforeseeable ways in future atmospheric studies. The data were gathered as part of the National Hail Research Experiment, managed by the National Center for Atmospheric Research and sponsored by the Weather Modification Program, Research Applications Directorate, National Science Foundation.

Charles A. Knight
June 1978

ACKNOWLEDGMENTS

The contribution of the University of Wyoming, and particularly G. Vali, in obtaining and making available the 10UW aircraft data is greatly appreciated. The NCAR Research Aviation Facility made available the 304D aircraft data. J. C. Fankhauser, A. J. Heymsfield and C. A. Knight made helpful comments on the manuscript.

CONTENTS

Foreword iii

Acknowledgments v

List of Figures ix

Abstract xi

I. METEOROLOGICAL SYNOPSIS 1

II. RADAR HISTORY 7

III. PENETRATING AIRCRAFT 11

A. Sailplane Penetration 11

B. 10UW Penetrations 19

IV. OTHER DATA 32

A. Mesonetwork 32

B. Doppler 32

C. Time-Lapse Photography 32

D. Still Photographs 32

V. SUMMARY 34

APPENDICES

A. Grover Radar Specifications 36

B. Sailplane Instrumentation 38

C. Wyoming Queen Air 10UW Instrumentation 45

REFERENCES 49

LIST OF FIGURES

Figure	Title	Page
1	Surface analysis on 22 June 1976	2
2	500 mb analysis	3
3a	Grover 1439 sounding	4
3b	Potter (modified) 1450 sounding	5
4a	Radar PPI of storm structure at 14:30:25	8
4b	Same as 4a except at 15:00:41	9
4c	Same as 4a except at 15:30:40	9
4d	Same as 4a except at 15:53:58	10
4e	Same as 4a except at 16:35:30	10
5	Radar PPI of storm structure and sailplane-investigated area at 15:25:57	12
6a-c	Sailplane and 10UW tracks on small-scale radar PPI	13
7	Time-height profile of maximum reflectivity in sailplane-penetrated cell	15
8	Sailplane data plots from 1520 to 1530	16
9	Radar PPI of storm structure and sailplane-investigated area at 15:42:16	18
10	Sailplane data plots from 1535 to 1550	20
11a-g	10UW data and flight tracks for seven penetrations between 1520 and 1555	22
12	Photograph of developing southwest flank of the storm complex	31

ABSTRACT

The NOAA/NCAR sailplane penetrated a growing turret on the west side of a developing echo system prior to the time of the radar "first echo" at the sailplane's altitude. This storm element was located on the southwest flank of a major storm complex, the same area where many earlier developments had evolved and subsequently moved northward through the general storm mass. The sailplane made two and a half spirals in the same location relative to the turret updraft, which was about 1.5-2.0 km in diameter. During the 7 minute in-cloud period (15:21:30 - 15:28:30), the sailplane encountered strong updrafts (maximum 22 m sec^{-1}) and increasing ice particle concentrations with time. Radar support was insufficient in providing a total reflectivity history about the sailplane's cloud penetration. The maximum reflectivity encountered by the sailplane was 15-20 dBZ_e. Particle camera data indicated that precipitation-sized particles were exclusively ice; no liquid drops greater than cloud droplet size were detected.

Seven cloud passes at 5.0-5.5 km MSL were made by Wyoming Queen Air 10UW in the same general area as the sailplane's penetration. Data collected between 1520 and 1555 showed a persistent updraft region on the western flank of the developing cell, and documented the presence of graupel during this period, some apparently in updraft regions.

I. METEOROLOGICAL SYNOPSIS

Figure 1 shows the surface synoptic conditions present at 1200 MDT, about the time of initial convection in the NHRE area. Significant features include a weak cold front, a dry line (or lee trough), and a strong low-level flow of moist air from the southeast. The cold front lies across the southeast corner of Wyoming, and the airmass behind it is marked by slightly cooler temperatures and southwesterly winds. The dry line separates the dry air and southerly winds along the front range of the Rockies from the moist air and southeasterly winds across Kansas and Nebraska. The 15°C isodrosotherm lies close to the dry line which is approximately through Grover, Colorado, and satellite photographs show a line of convection forming along this well-marked boundary. Convection is already active in the western panhandle of Nebraska.

The 500 mb analysis on the morning of 22 June (Fig. 2) shows difluence of the weak southwesterlies over the NHRE area. Denver reported a geopotential height fall of 40 m during the previous 12 hours, and had an additional fall of 30 m during the next 12 hours in response to a large amplitude trough moving eastward through the western U.S.

The closest sounding, temporally and spatially, to this first echo case was the Grover 1439 MDT release. It is plotted in Fig. 3a with the θ_e profile in the upper left insert. Figure 3b is the mature storm case study's representative sounding on this day, which is the 1450 Potter sounding modified below cloud base by aircraft data. NCAR Queen Air 304D descended to near the surface at 1617-1622 in the inflow region southeast of the main storm complex (approximate Grover coordinates are

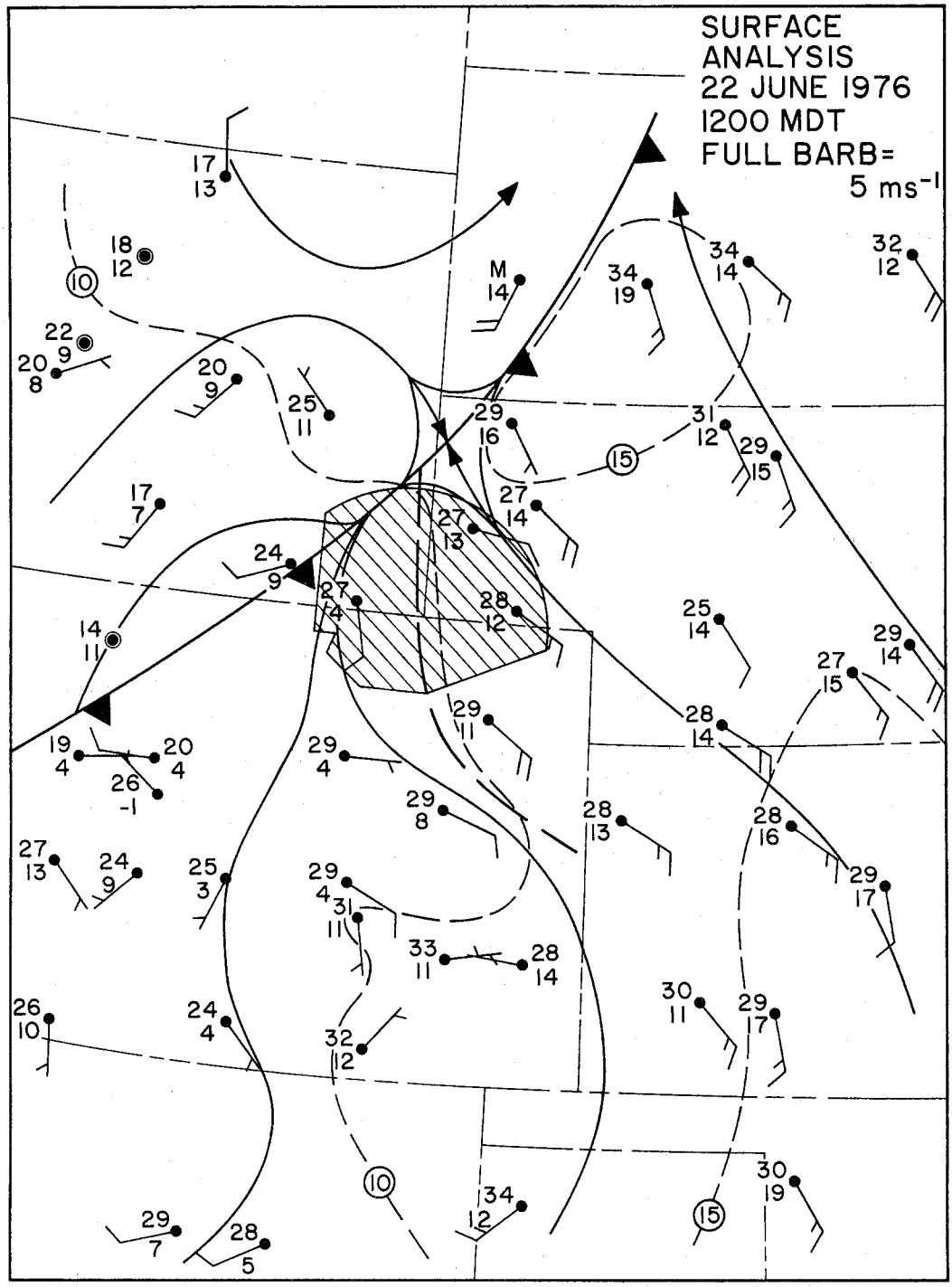

Fig. 1. Regional surface map for 1200 MDT on 22 June 1976 showing the synoptic scale conditions at about the time of initial convection in northeastern Colorado. The NHRE airspace for aircraft operations is the shaded area. Temperature, dewpoints, and wind speed and direction are plotted at each station. The dashed lines are isodrosotherms of 10°C and 15°C. Heavy dashed line is the dry line boundary.

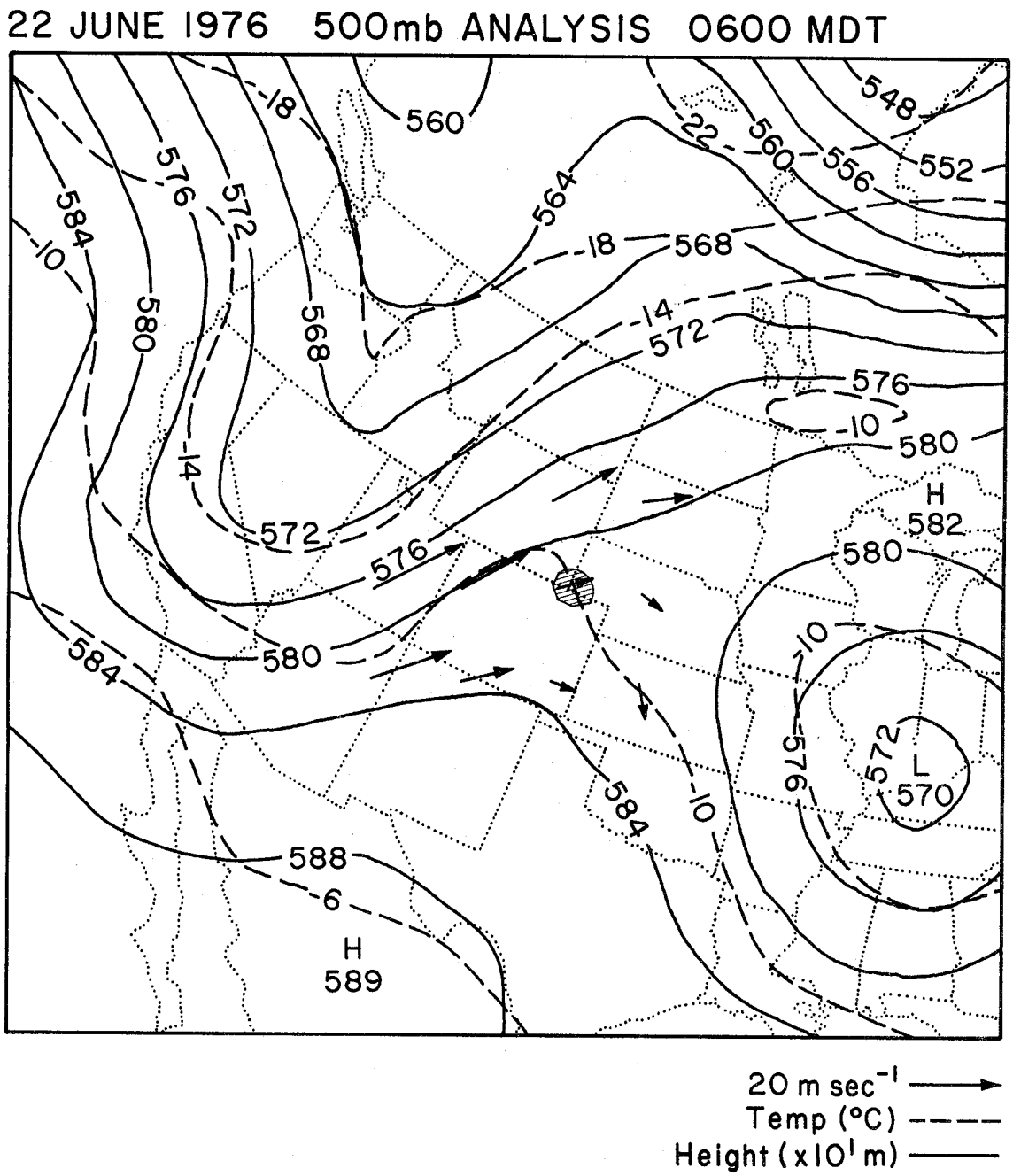

Fig. 2. 500 mb map of the western half of the U.S. for 0600 MDT on 22 June 1976 showing the early morning midlevel synoptic conditions. Solid lines are geopotential height contours (x10 m) every 40 m; dashed lines are isotherms (°C) every 4°C; and wind vectors are plotted around the NHRE airspace (shaded area).

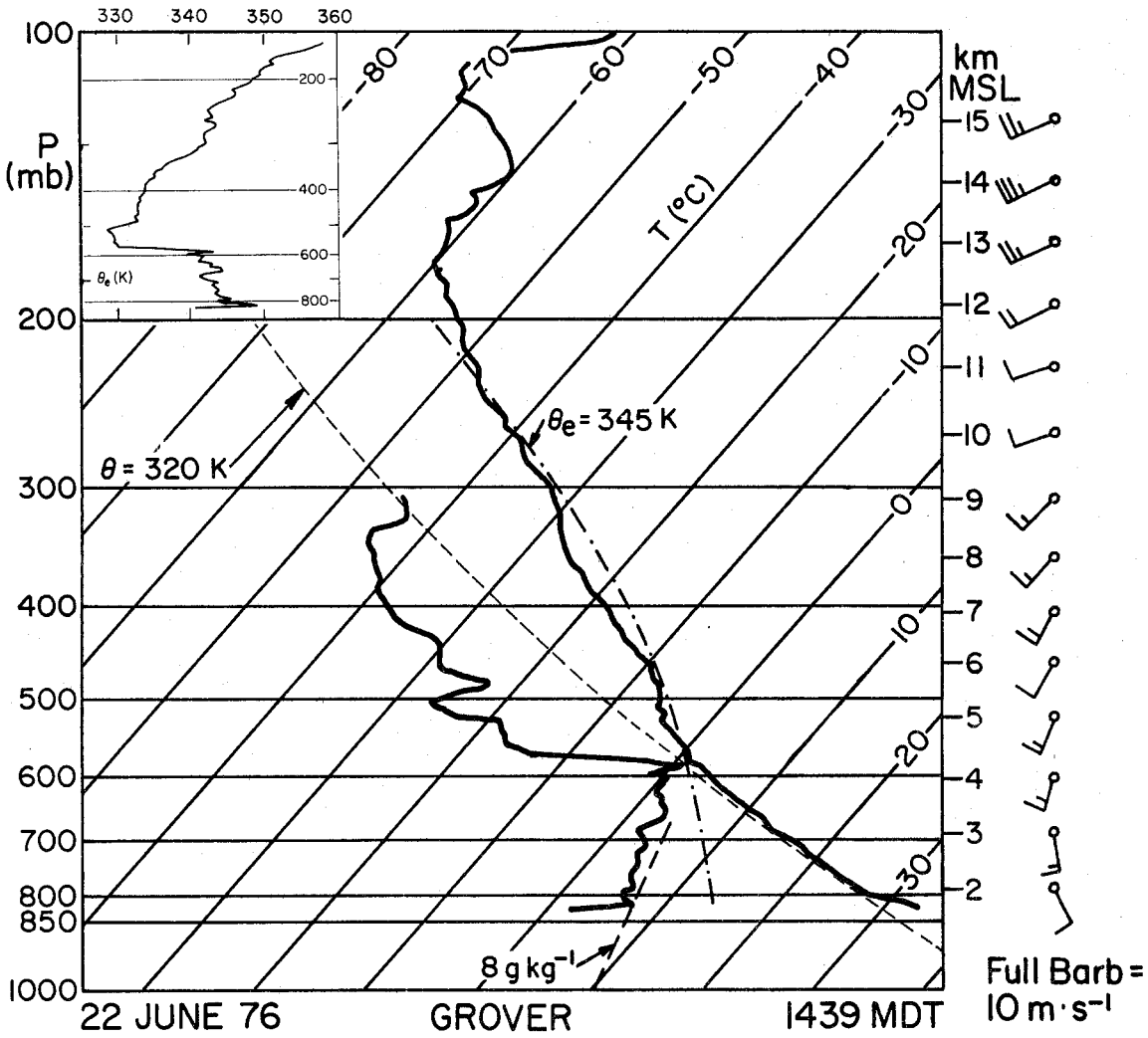

Fig. 3a. Thermodynamic diagram showing the vertical distribution of temperature and dewpoint from Grover 1439 sounding. Selected dry and moist adiabats and mixing ratio have been plotted as dashed lines and labeled. Winds are plotted every kilometer; full barb is 10 m sec^{-1}. Insert in the upper left shows θ_e vs. pressure for this sounding.

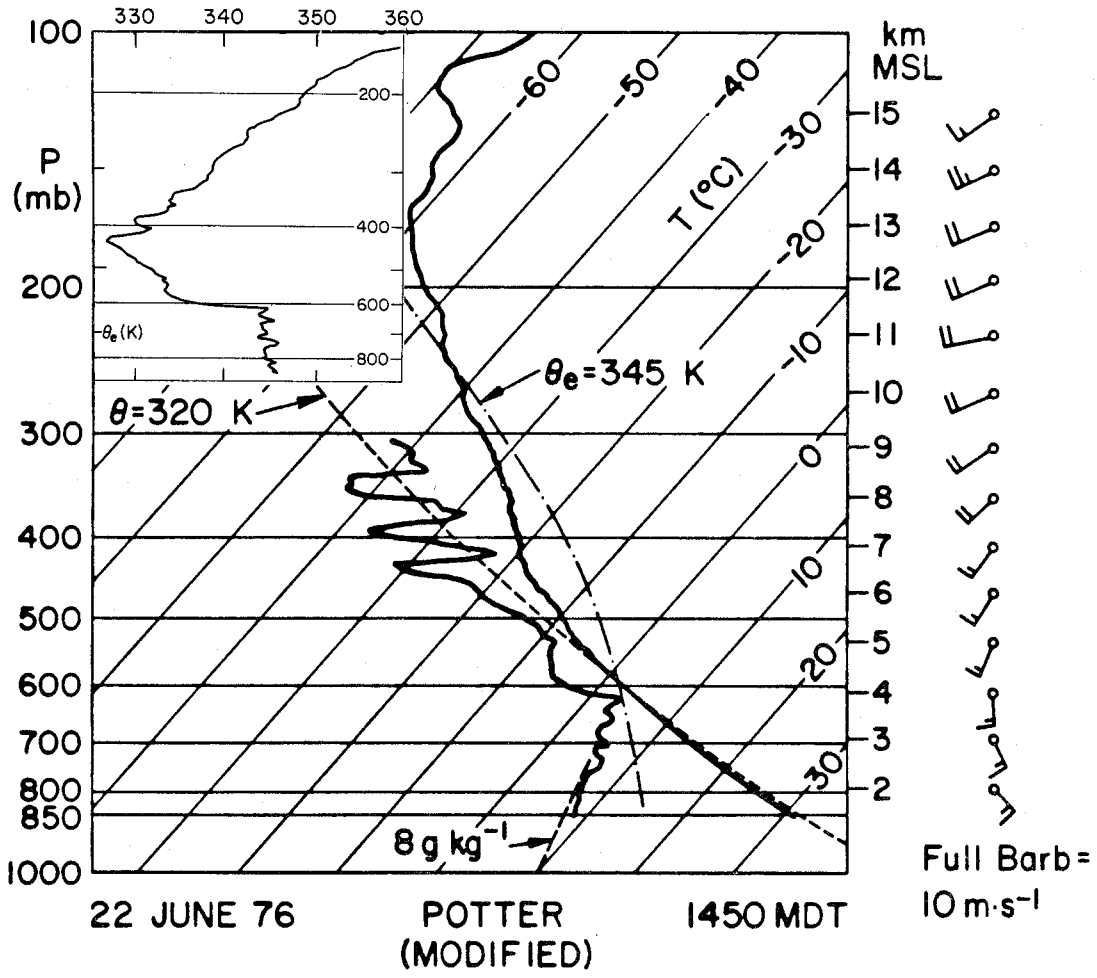

Fig. 3b. Same as Fig. 3a except from Potter 1450 sounding, modified below 605 mb by values from 304D descent sounding at 1617-1622 in the storm inflow region (position is plotted in Fig. 4c).

32.5, -15.0; see Fig. 4c), and the aircraft values are substituted for the Potter values in the lowest 250 mb of the sounding. The two major differences are lower θ values at Potter and the lower mixing ratio at Grover. While mesonetwork data near and at Grover indicate that the θ values are slightly high in that sounding, they substantiate the slightly drier air in the southwest corner of the network, which is the first echo area. A pass near cloud base under the southwestern area of the storm complex at approximately 1605 was made by both NCAR Queen Airs, giving updraft θ_e values of about 344°K and pressure at the LCL of 600-605 mb. θ_e values in the southwest corner of the mesonetwork were generally 344-345°, which further supports a typical feature of inflow-updraft conditions in northeast Colorado of a dry adiabatic lapse rate and relatively constant mixing ratio to cloud base.

II. RADAR HISTORY

Figures 4a through 4e show radar reflectivity (Z_e) data in PPI format indicating the general echo development during the period of interest.[1] At 1430 (Fig. 4a), a north-south line of discrete storms had formed over the bluffs about 10 km east of Grover and near the dry line shown in Fig. 1. By 1500 (Fig. 4b) the storms had organized into a more continuous line but were still discrete. Movement of the line was very slowly eastward, while new storm cells formed at the south end, just southeast of Grover, and propagated northward during their life cycles. Figure 4c is the reflectivity structure at about the same time that the sailplane investigated growing turrets on the western flank of a new storm cell, marked with an arrow on the PPI. Figure 4d shows the storm cell as it developed and moved north-northeastward into the general storm mass. Around 1600, the outflow from the earlier storms became sufficiently organized to be detected by the mesonetwork. The northern end of the line began to diminish in intensity while the southern end developed into a large multicellular complex which was investigated in detail in the mature storm case study between 1600 and 1700. This change of character is reflected in the echo structure in Fig. 4e at 1635.

[1] All radar data plots have the Grover radar at the origin of the coordinate system.

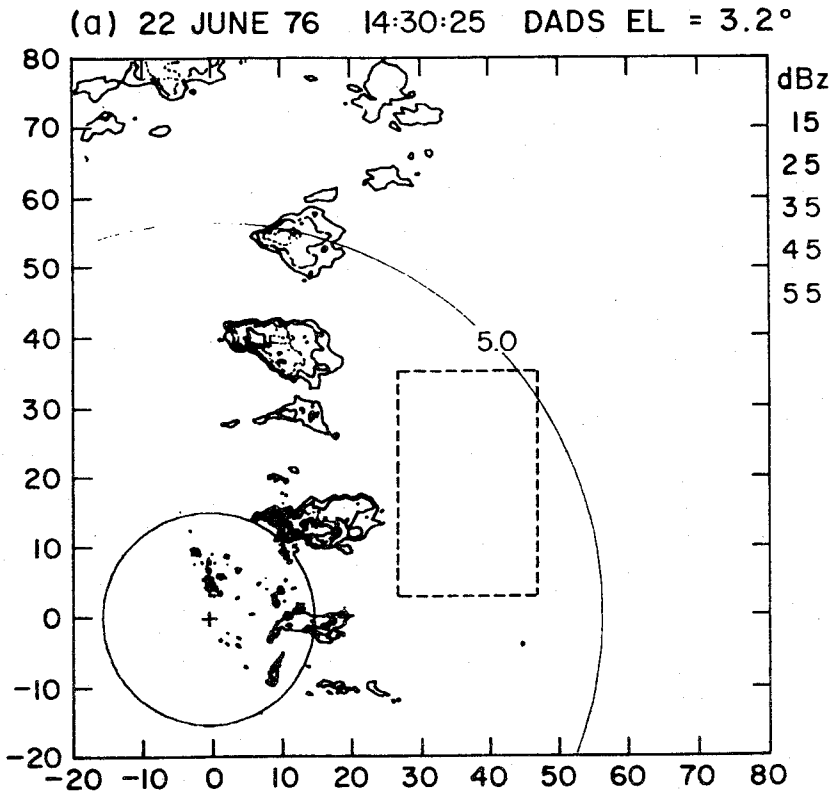

Fig. 4a. The 14:30:25 PPI radar scan on 80 x 80 km map showing radar reflectivity contours at 3.2° elevation angle on 22 June 1976. Contours are in 10 dBZ_e intervals beginning at 15 dBZ_e. A constant altitude circle is at 2.5 km and an arc is at 5.0 km. Cross is position of Grover radar and dashed rectangle is the boundary of the dense precipitation network.

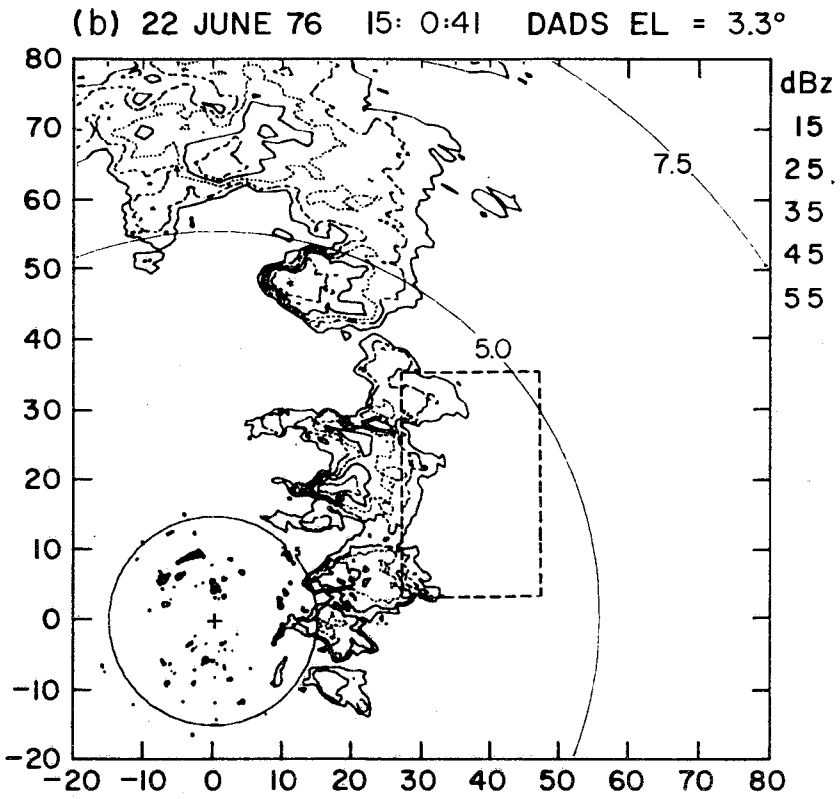

Fig. 4b. Same as 4a except at 15:00:41 and 3.3° elevation angle. The 7.5 km constant altitude arc has also been added.

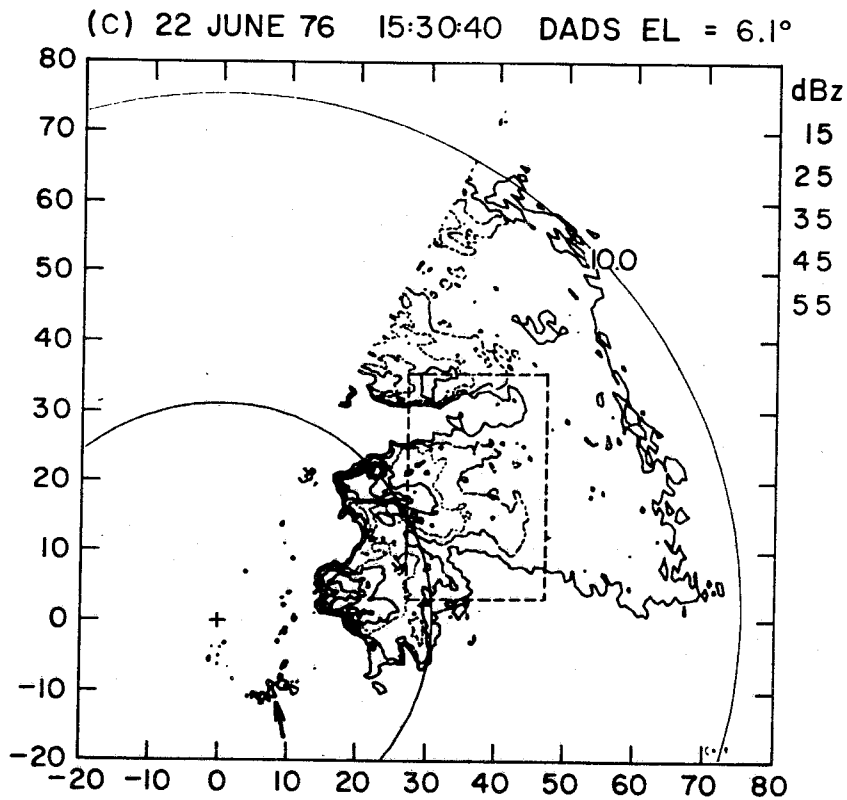

Fig. 4c. Same as 4a except at 15:30:40 and 6.1° elevation angle. Constant altitude arcs are now at 5.0 and 10.0 km. Arrow at approximate coordinates (10, -10) identifies beginning echo of cell investigated by the sailplane.

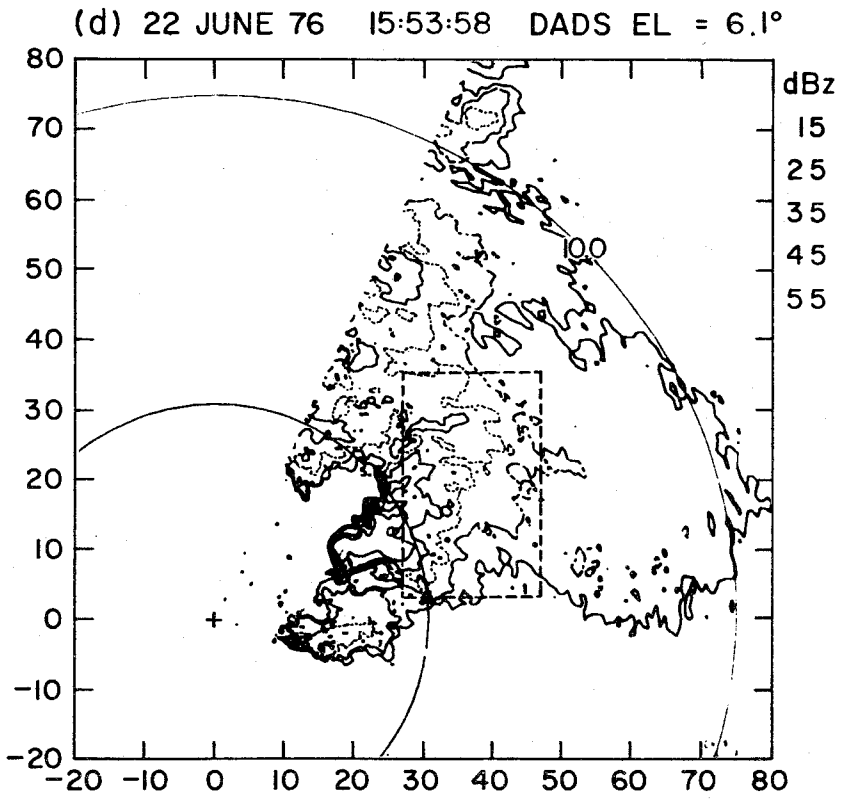

Fig. 4d. Same as 4c except at 15:53:58.

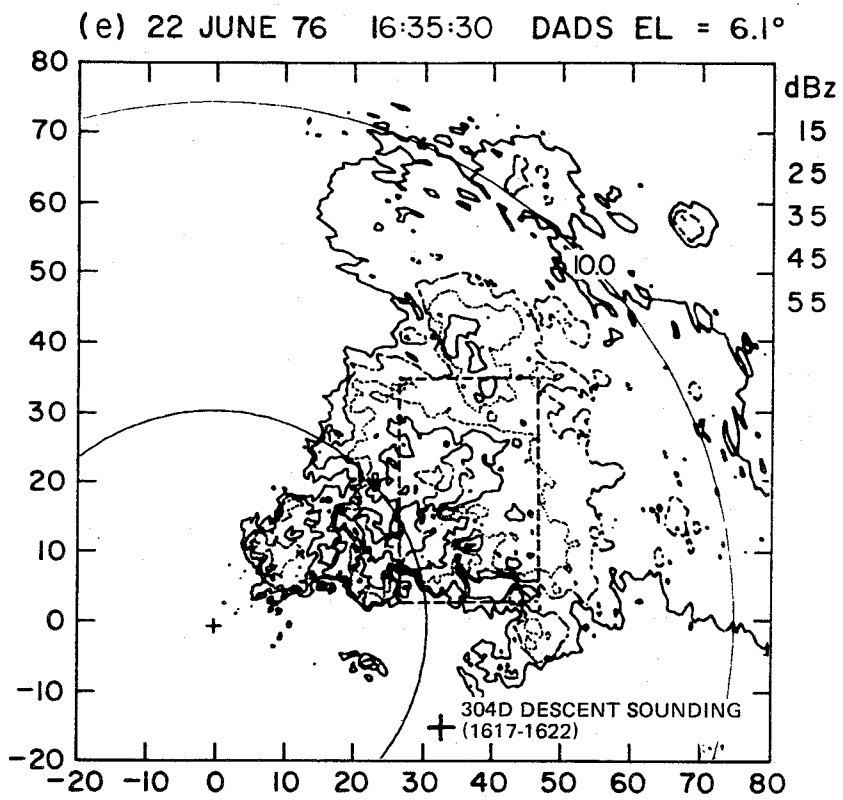

Fig. 4e. Same as 4c except at 16:35:30. Position of 304D descent sounding is indicated by cross at (32.5, -15).

III. PENETRATING AIRCRAFT

A. SAILPLANE PENETRATION

The first echo case centers around a penetration by the NCAR/NOAA sailplane of a turret on the western edge of a developing storm cell southwest of the main storm complex. While initially in reflectivity regions less than -5 dBZ_e, subsequent spiralling in the cloud moved the sailplane closer to higher reflectivity regions. This was a consequence partly of the echo area expanding with time, and partly of the sailplane's gain in altitude. Figure 5 is the PPI at the time of the sailplane penetration. The box in the lower left-hand portion of this figure indicates the approximate echo area presented in the time sequential figures 6a, b and c. These figures show the sailplane's track from 15:21:00 to 15:28:30 and three segments of the University of Wyoming's Queen Air 10UW track from FAA data. The X's on the tracks are positions at the time of the radar scan, while all other positions are corrected for a cell motion of 10 m sec^{-1} to the northeast. The track of the sailplane is also shifted 1 km farther in range (from Grover) to match the CP-2 radar "skin paint" of the sailplane observed on three different occasions. The two occurrences of "skin paint" on 10UW during the first echo portion of its flight did not show a consistent trend for correcting the FAA track, and suggests a track accuracy of ±1.5 km.

Since the maximum elevation angle of the CP-2 radar during this period was 17.4°, the maximum altitude of radar data at the area of interest (range ∿15 km) is 6.0-7.0 km MSL.[2] In Fig. 6a the sailplane

[2] All altitudes are mean sea level unless otherwise stated.

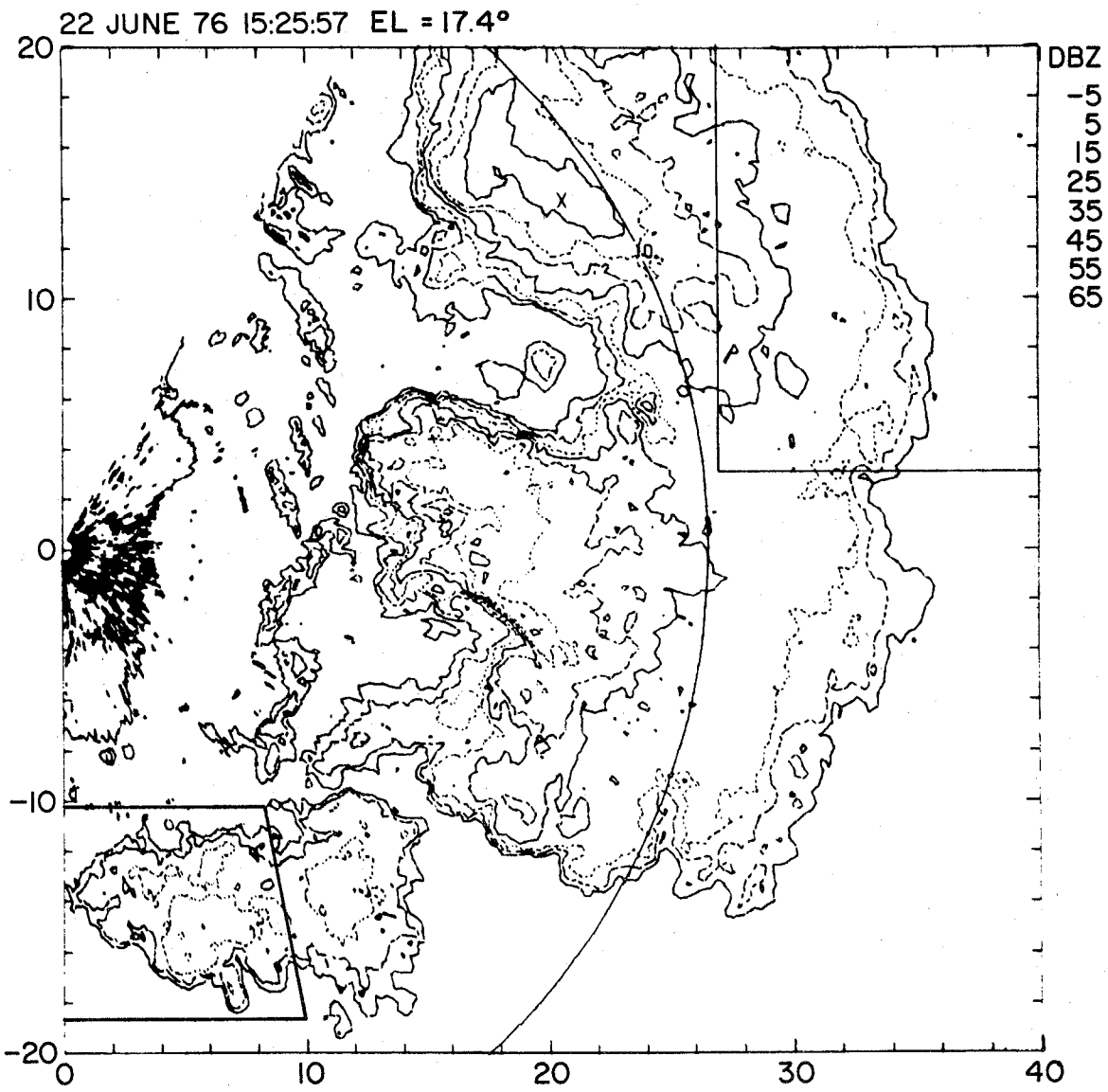

Fig. 5. The 15:25:57 PPI radar scan on 40 x 40 km^2 map showing radar reflectivity contours at 17.4° elevation angle. Contours are in 10 dBZ$_e$ intervals beginning at -5 dBZ$_e$. The constant altitude arc is at 10 km, and the southwest boundary of the dense precipitation network is plotted as a rectangle in the upper right of the figure. The boxed area in the lower left designates the expanded area plotted in Fig. 6.

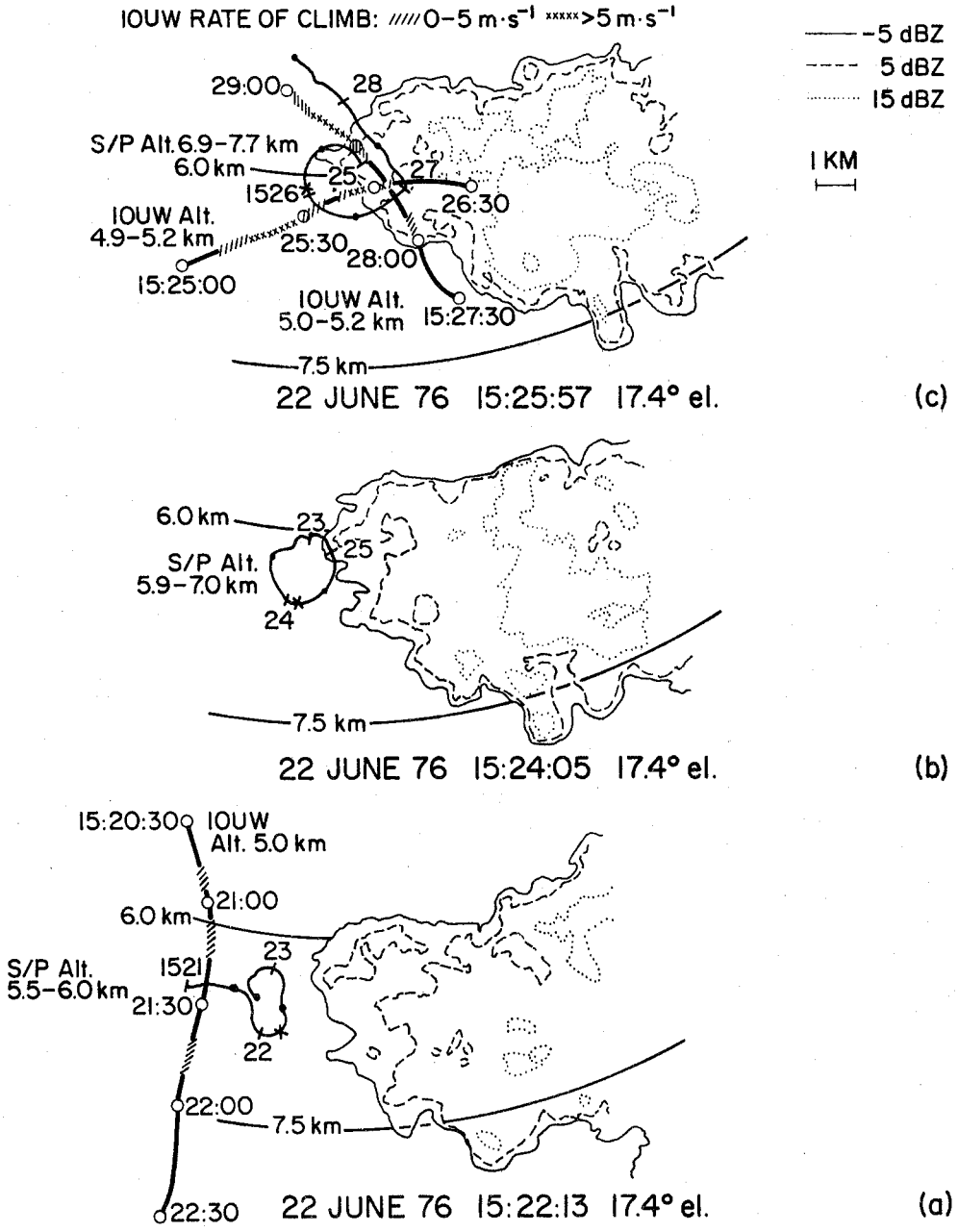

Fig. 6. Radar PPI's of the expanded area identified in Fig. 5, with the sailplane corrected track (solid line) and 10UW partial track (heavy solid line) plotted and altitude ranges labeled. Sailplane position is marked every 30 sec, labeled every minute, and X at time of PPI. 10UW position is marked and labeled every 30 sec, and hatched and cross-hatched when rate of climb is 0-5 m sec^{-1} and >5 m sec^{-1} respectively. Reflectivity contour intervals are 10 dBZ$_e$ apart beginning at -5 dBZ$_e$, and constant altitude arcs are drawn at 6.0 and 7.5 km.

is close to the level of the PPI plane while in Figs. 6b and c it is higher than the PPI plane. Except for a small amount of CP-4 data, it is not possible to know what is happening above the sailplane or even at the peak of its climb with respect to reflectivities. Figure 7 is the reflectivity history of the cell into which the sailplane penetrated. The critical gap in radar data is between 1520 and 1527 above 6.5 km. By noting the spread of the 15 dBZ_e contours in Fig. 6, it can be seen that the reflectivity area of the cell is rapidly expanding during this period, which may indicate either rapid particle growth or fallout of particles from above.

The sailplane data (altitude, temperature, vertical airspeed, J-W liquid water content, integrated FSSP LWC, FSSP droplet concentration and mean droplet diameter, and indications of cloud particle camera images) during this penetration are presented in Fig. 8. Noteworthy features are the strong updrafts (maximum at ∿152425 of 22 m sec^{-1}) and high liquid water contents in those updrafts, which were strongest at the southern end of the sailplane's spirals. The temporal continuity of the updraft is supported by the 10UW rate of climb indications, and by a weak reflectivity region that is evident in this main updraft area. Graupel and ice particles increase during each spiral, and the last (half) spiral has especially sharp gradients of liquid water content and vertical airspeed. The J-W LWC measurements seem to be reliable during this and later penetrations, judging from correlation with the vertical airspeed and θ_e values. There is no obvious deterioration in the J-W measurements which is apparent in some cases when the J-W strut collects so much ice that this build-up interferes with the measurements.

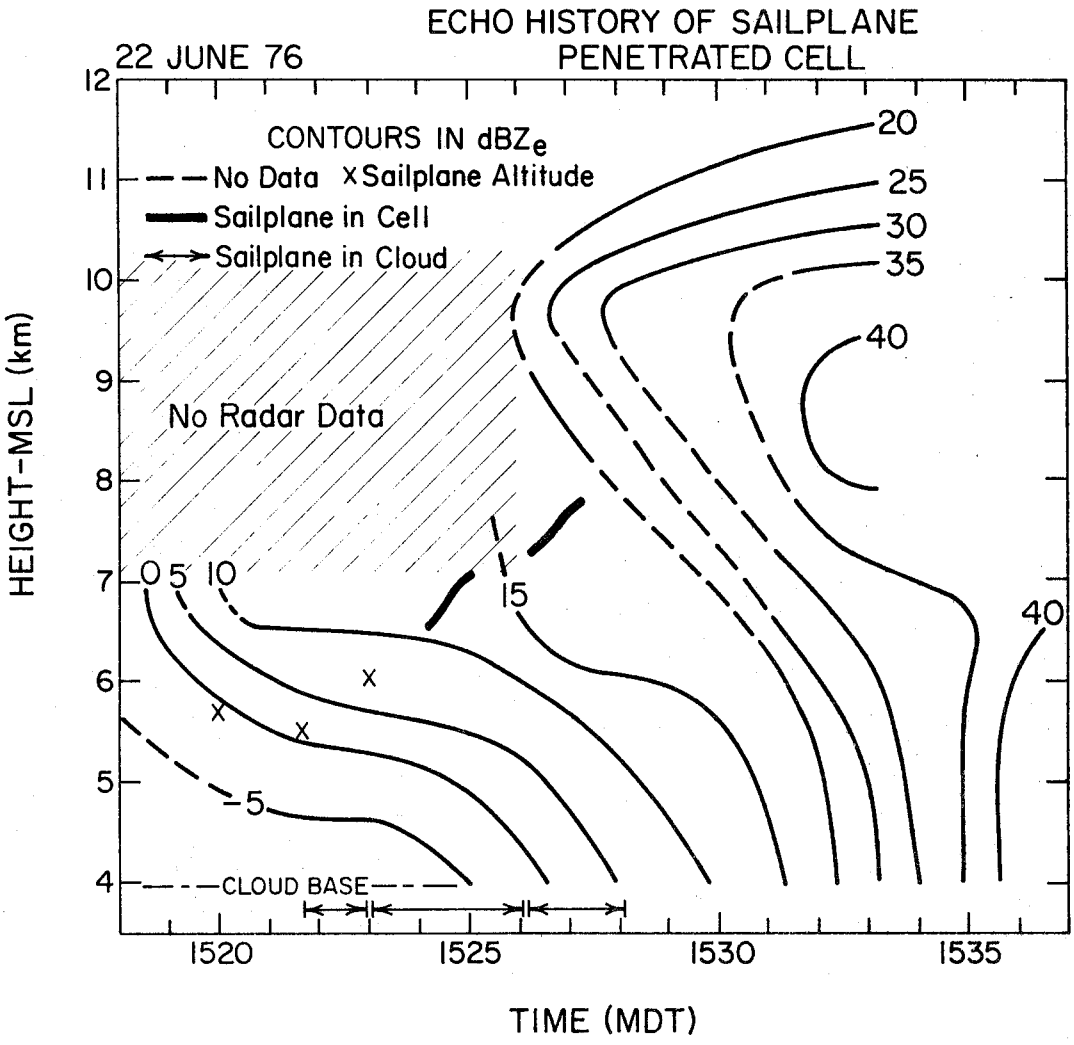

Fig. 7. Time-height profile of reflectivity contours for the sailplane penetrated cell at 5 dBZ_e intervals above -5 dBZ_e. The dashed lines and shaded area indicate areas of no radar data. Sailplane altitude and in-cell times are marked by X's and extra heavy lines respectively. In-cloud periods are indicated by arrows just above the lower axis.

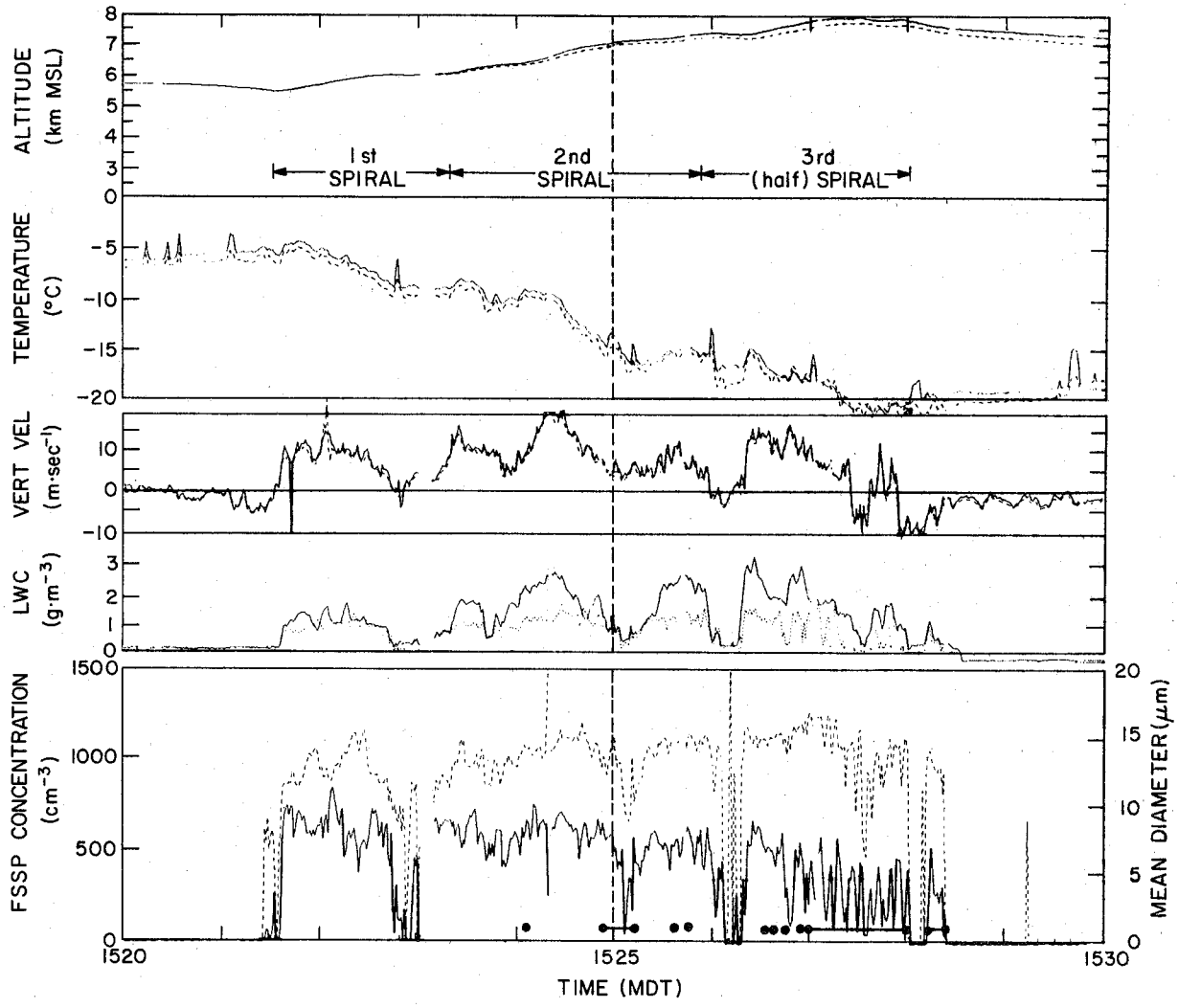

Fig. 8. Sailplane data from 1520 to 1530 showing altitude, temperature, vertical airspeed, liquid water content and FSSP concentration and mean diameter from the first penetration on 22 June 1976. For altitude, the solid line is from the Hamilton Standard pressure transducer and the dashed line is from the variometer. For temperature, solid is from the reverse flow probe, and dashed is from an exposed "window" probe. For LWC, solid is from J-W probe, and dashed is from FSSP integrated spectra. For FSSP plots, solid is total concentration with scale on the left axis and dashed is mean diameter with scale on the right axis. First, second and third (half) spirals are indicated below altitude plot, and times of ice particle image detection are denoted at the bottom by dots (single events) and lines (continuous events).

The J-W values agree reasonably well with the LWC calculated from the FSSP data during the early part of the penetration, but deviate markedly later in the penetration. This was a consequence both of the FSSP icing up and of the fact that the FSSP registers spurious counts of larger drops when many ice particles are present. In the updraft during the sailplane's first spiral, the FSSP measured average droplet concentrations of $\sim$650 cm^{-3} with a mean diameter $\sim$16 μm, while in later and stronger updrafts, the concentrations were lower. This is a typical indicator of FSSP problems. The cloud particle camera images indicated that graupel and out-of-focus particles with some identifiable rimed dendrites were the dominant particle forms. The largest relative concentration of identifiable (in-focus) particles was at about 15:27:15 - 15:27:30, when the sailplane was above the highest reflectivity (15 dBZ_e) of the penetration (see Fig. 6c). However, this maximum concentration was still fairly low ($\leq$ 5 ℓ^{-1}). Although the resolution of the CP-4 data output is not good, there is an indication that the 15 dBZ_e contour extended above the sailplane at this time and place (as noted in Fig. 7).

An attempt was made between 1536 and 1550 to penetrate turrets which 10UW was sampling. However, the sailplane investigation was north of the 10UW penetrations during this time period. Figure 9 shows the storm's structure on a radar PPI with the sailplane track plotted on the expanded portion. The track has again been corrected about 1 km in range to bring it in agreement with the CP-2 positions, and has had a storm motion of 8 m sec^{-1} to the northeast subtracted from it. Hence, the track at the early and late times may differ from true position by more than a kilometer while in the middle of the period it should be

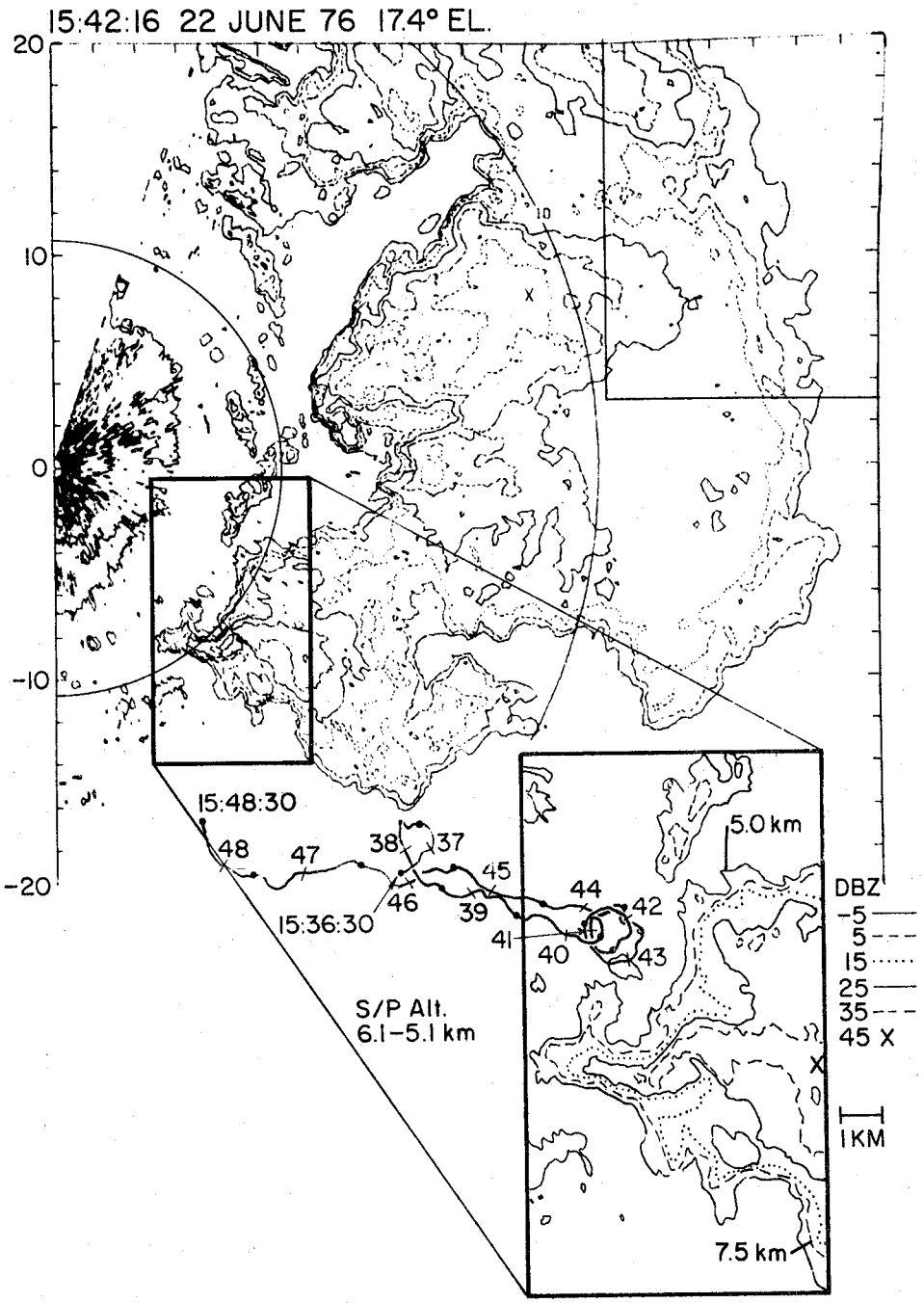

Fig. 9. Radar PPI at 15:42:16 and 17.4° elevation angle with contours in 10 dBZ_e intervals from -5 dBZ_e. Lower figure is expanded area of the upper figure showing the corrected sailplane track from 15:36:30 to 15:48:30. Track is marked every 30 sec and labeled every minute. Constant altitude arcs in the lower figure are drawn at 5.0 and 7.5 km.

within several hundred meters. It should also be noted that the sailplane is about one kilometer above the PPI plane in this figure. Figure 10 is the sailplane's data during this time period, and it can be seen that conditions were variable with weak up- and downdrafts and lower liquid water contents. This was apparently an inactive portion of the cloud. The particles imaged with the cloud particle camera were mostly out of focus. Identifiable particles were generally smaller and showed less riming than ice particles in the earlier penetration. Concentrations were also considerably lower.

B. 10UW PENETRATIONS

Wyoming's Queen Air 10UW made 7 cloud penetration passes during the first echo study period (1520-1555). The first three passes (S, T and U) were coincident with the sailplane penetration and are plotted on Figs. 6a-c with the sailplane track. Four other passes (V, W, A and B) were made in the same area providing good temporal coverage of the developing southwest flank at the 5.0 - 5.5 km level. 10UW had a failure of the dynamic pressure instrument on this day, and although clear air values were recoverable, in-cloud values were not. General information about updraft area and strength can be obtained from the aircraft rate of climb when the aircraft power setting is constant, but since airspeed is not available it must be used with caution. Data that are not highly dependent on airspeed were reduced using 80 m sec^{-1} as the true airspeed. These include pressure altitude, reverse flow temperature, hot-wire measured liquid water content, and particle data from the Particle Measuring System's ASSP and 2-D probes. These data are plotted for each pass in Figs. 11a-g. Included in these figures are the tracks of 10UW

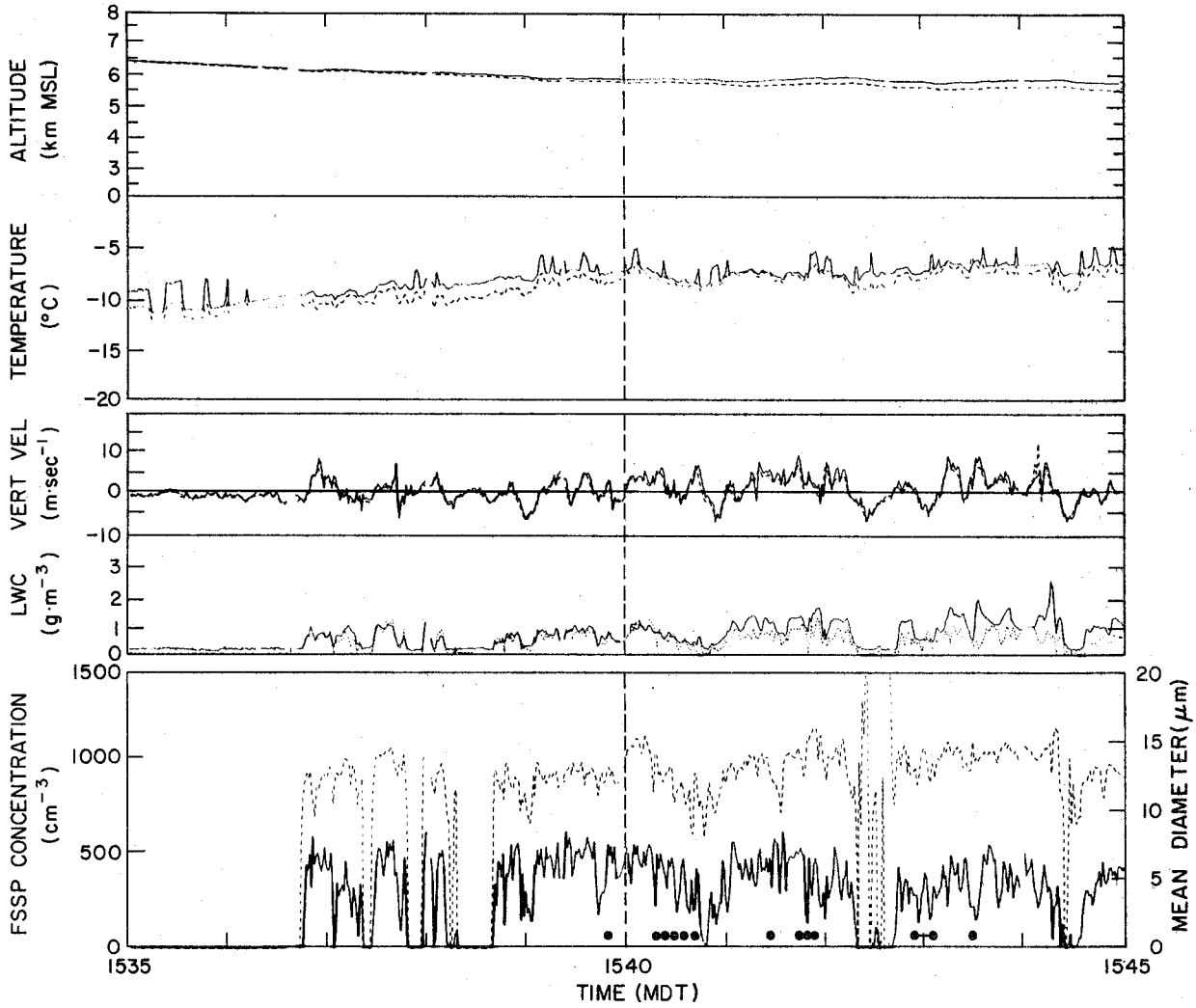

Fig. 10. Same as Fig. 8 except for the second penetration time period of 15:35:00 - 15:50:00 (Fig. 10 continued next page).

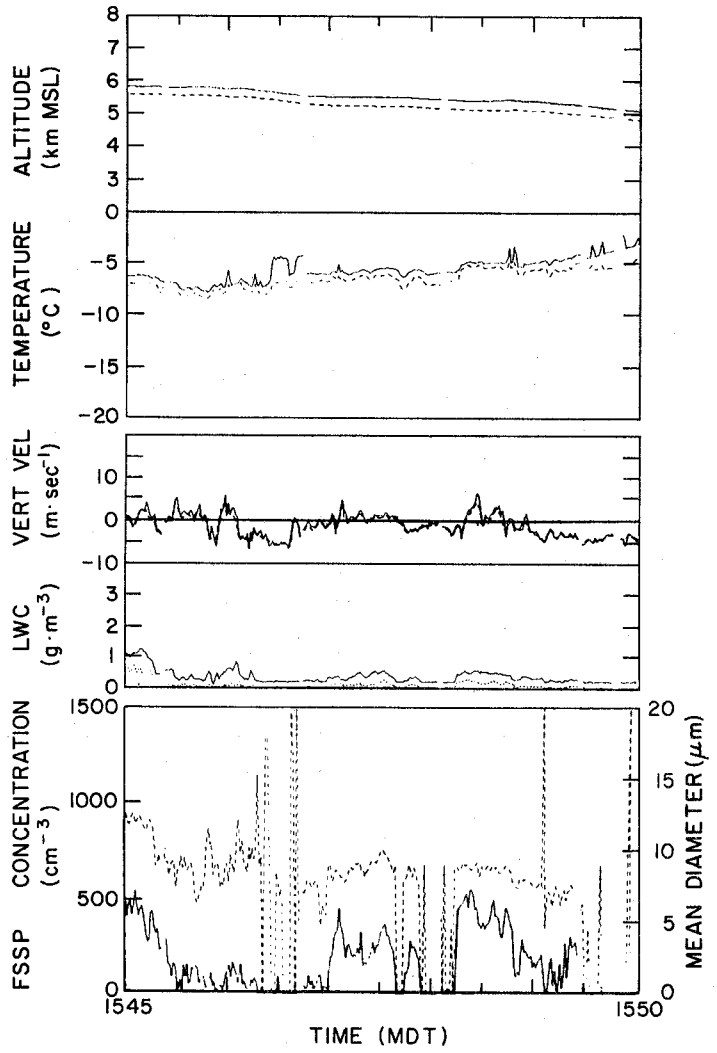

Fig. 10 (continued)

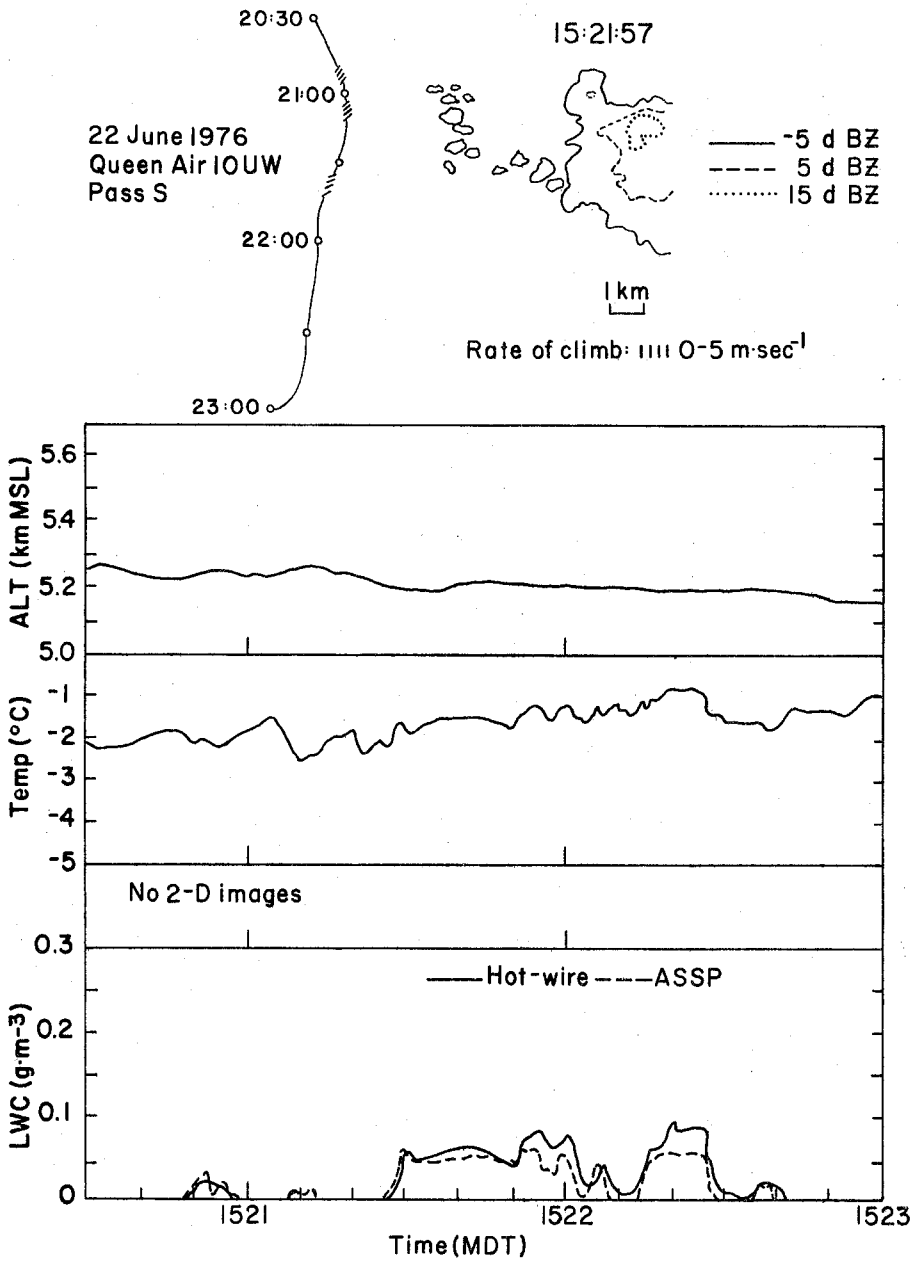

Fig. 11a. 10UW track and data from Pass S (15:20:30-15:23:00). At the bottom is the liquid water content from the hot-wire device (solid line) and ASSP integrated spectra (dashed line). Above that trace is the 2-D data characteristics, which showed no images on this pass. Next is the reverse flow temperature trace, and then the pressure altitude plot. The aircraft track, corrected from the PPI time (15:21:57) for a cell motion of 10 m sec^{-1} to the northeast, is plotted with the echo structure at about the time and height of the penetrations. Positive rates of climb are indicated on the aircraft track.

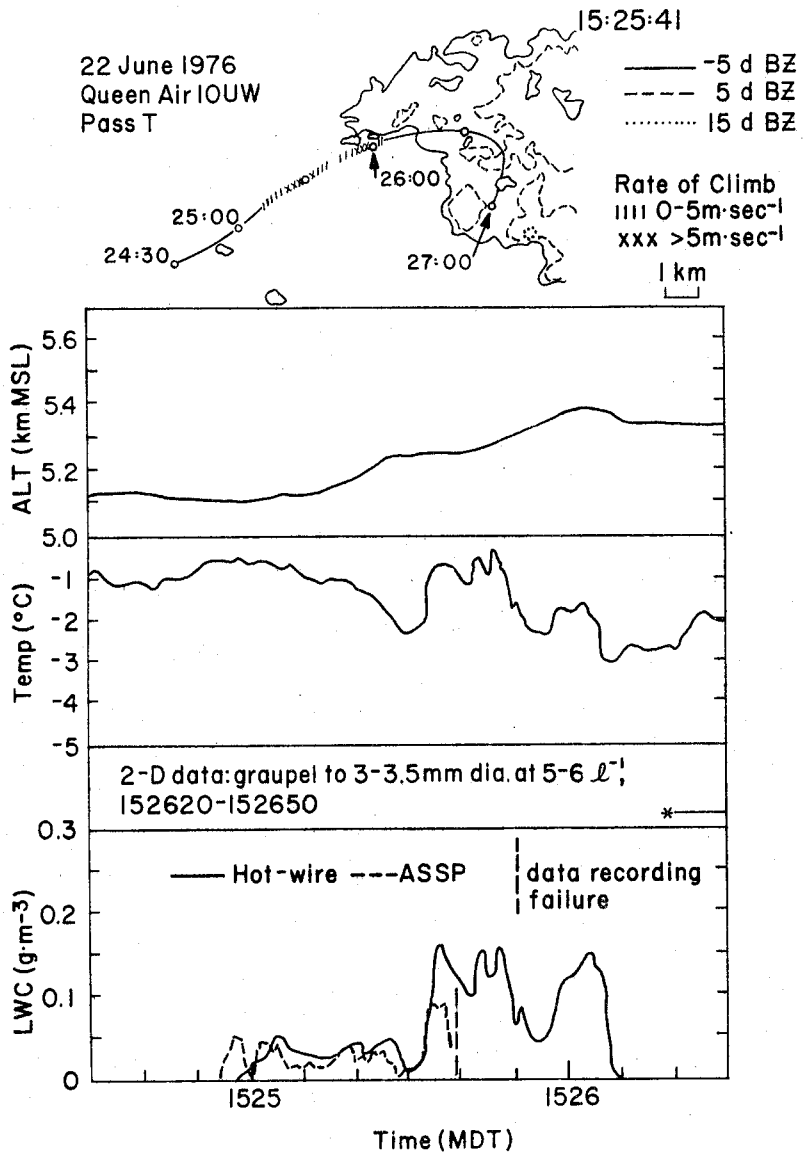

Fig. 11b. Same as Fig. 11a except for Pass T (15:24:30 - 15:26:30). Note data recording failure with ASSP.

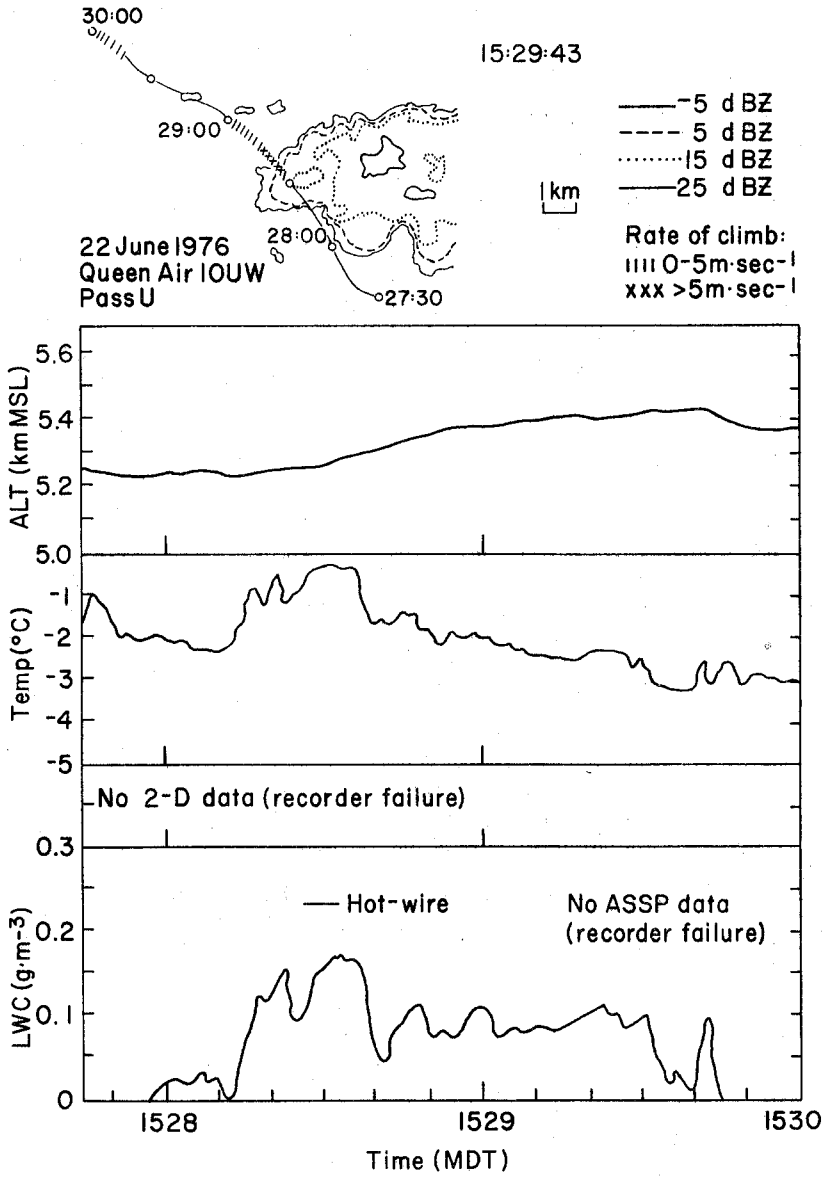

Fig. 11c. Same as Fig. 11a except for Pass U (15:27:45 - 15:30:00). No ASSP or 2-D data were available because the aircraft recorder malfunctioned during this period.

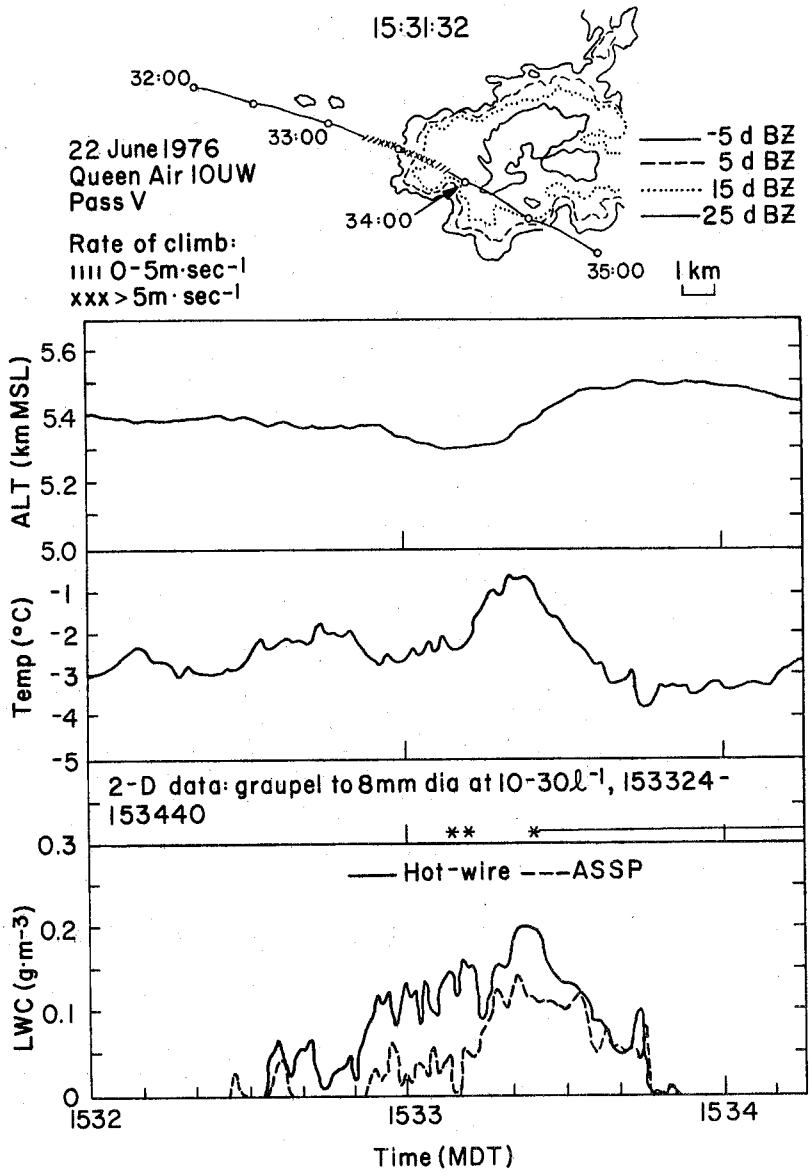

Fig. 11d. Same as Fig. 11a except for Pass V (15:32:00 - 15:34:15). Note that the PPI time is earlier than the penetration.

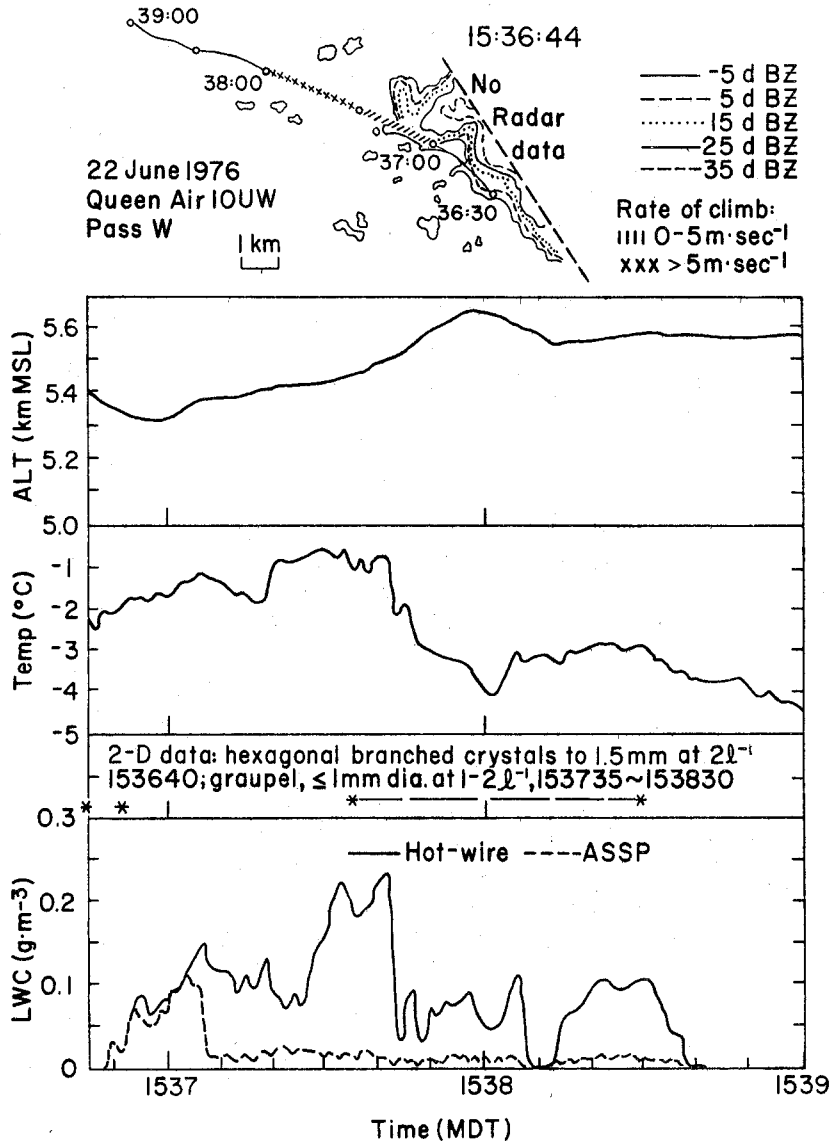

Fig. 11e. Same as Fig. 11a except for Pass W (15:36:45 - 15:39:00).

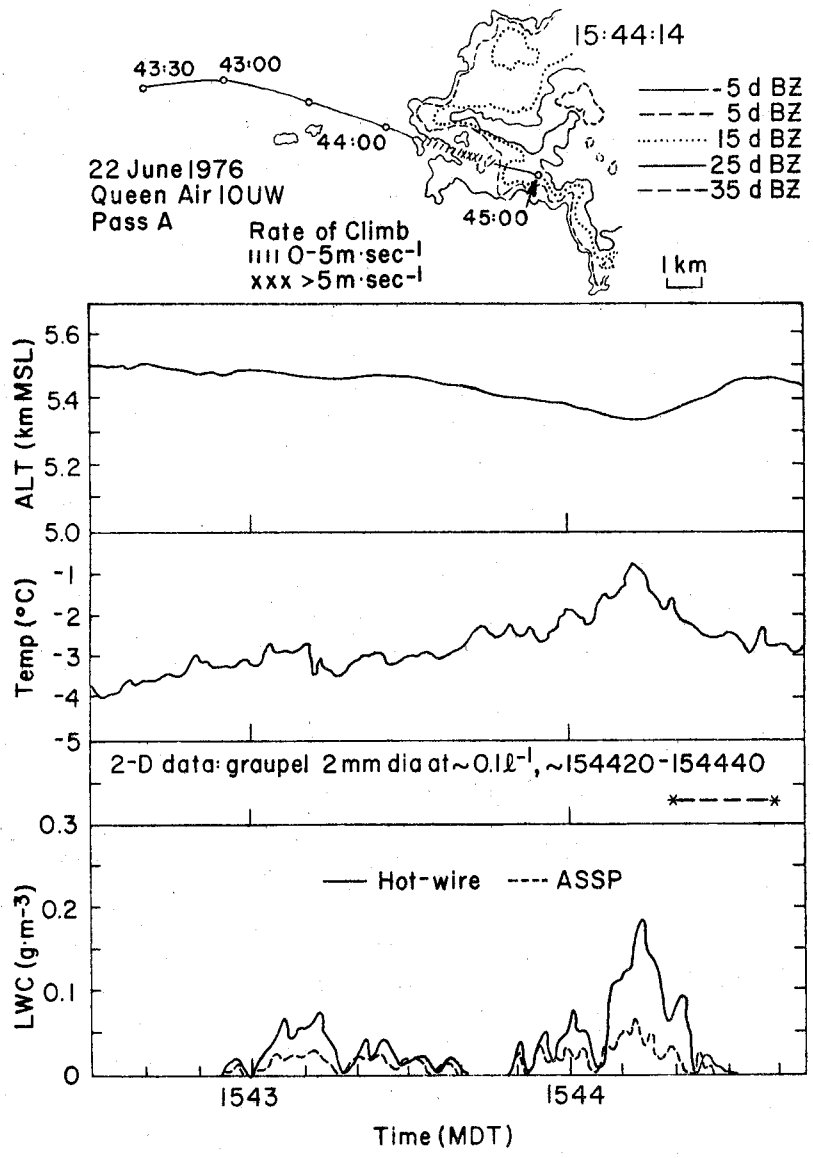

Fig. 11f. Same as Fig. 11a except for Pass A (15:42:30 - 15:44:45).

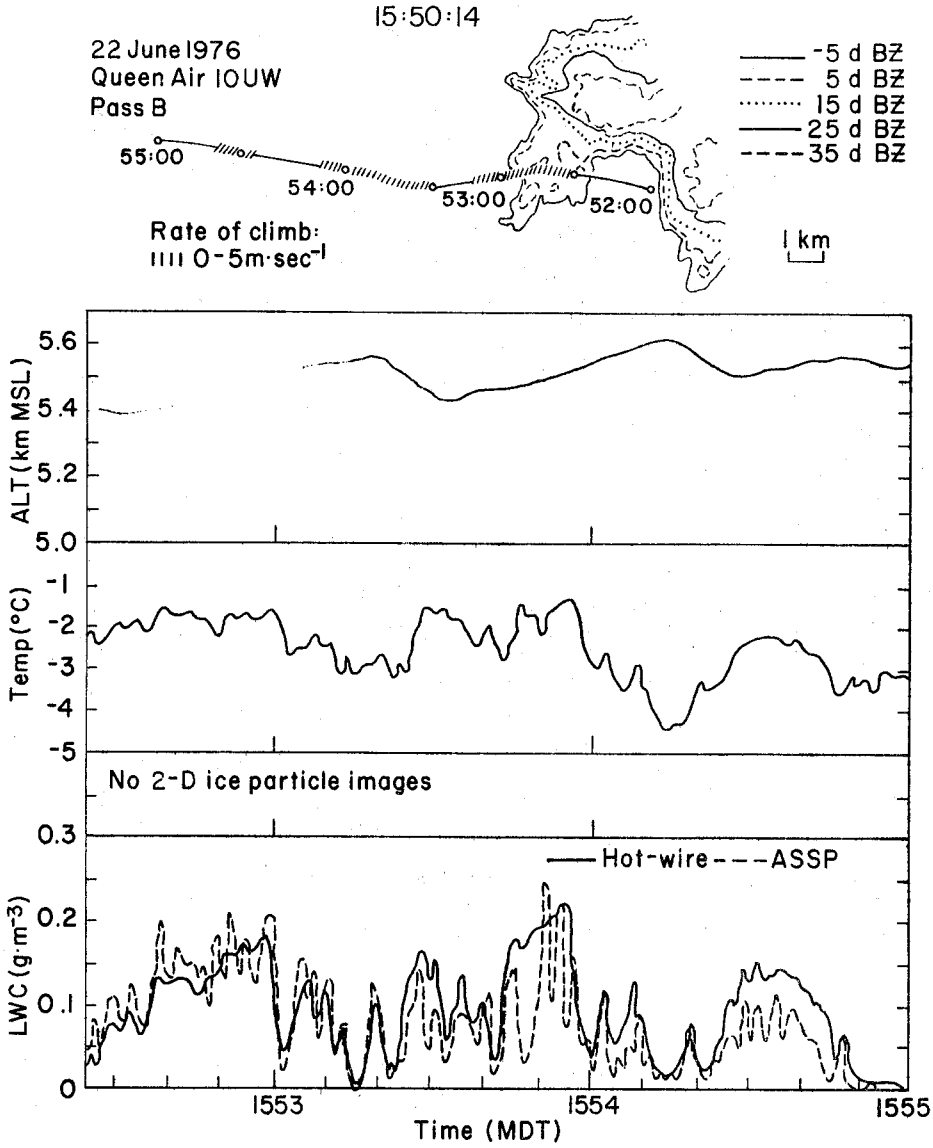

Fig. 11g. Same as Fig. 11a except for Pass B (15:52:25 - 15:55:00). Note that the PPI time is earlier than the penetration.

relative to the echo area on the southwest flank of the major storm complex. A cell motion of 10 m sec^{-1} to the northeast has been used, and the resulting track should be within 1.5 km of true position with respect to the cell. The PPI's presented in these figures show the reflectivity structure closest to 10UW's altitude and are in the range of 4.5 - 6.5 km. In passes V and B the PPI times were earlier than the flight leg, but they are the best available.

The accuracy of the temperature (using the fixed airspeed) should be within 1°C, with the resolution slightly worse than 0.1°C (see appendix) due to unknown airspeed fluctuations. The error in liquid water content measured with the hot-wire device is unknown, and the magnitude is unreliable. The ASSP concentrations should be within 10% of their "normal" values, but they are affected by the more serious particle coincidence problem discussed in the sailplane instrumentation appendix. This error can cause gross underestimates of droplet concentrations: hence, liquid water content derived from the integrated spectra would also be grossly underestimated. The coincidence error is not corrected in these data. Although the magnitudes of the hot-wire and ASSP-derived LWC are inaccurate, the data are presented to show the locations of cloud water and to compare their fluctuations with other data. A brief summary of the 2-D data is presented in the figures showing the time period in which ice particles were detected and their maximum sizes and concentrations.

The seven penetrations by 10UW were in the same general location with respect to the growing echo region. The rate of climb data indicate the continual presence of updrafts to the west of the echo area,

although they were not more than a few kilometers in length along the flight track. Most ice particles were identified as graupel and they coincided fairly well with aircraft penetrations of the echo area. Liquid water appeared to be depleted by the presence of ice in most of the passes. Although the rate of climb indications are rough estimates, it is noteworthy that ice particles were detected in updraft areas in passes V, W and A, with concentrations of 10-30 ℓ^{-1} in pass V.

The 10UW passes support the sailplane observations in detecting a persistent updraft region under the area investigated by the sailplane, and in documenting the presence of graupel in many of the passes. However, because of the cellular nature of this developing region, the origin and spread of precipitation-size particles is more complex than just two aircraft can resolve.

Figure 12 is a photograph taken from the sailplane of the southwest flank of the main storm mass where the sailplane and 10UW penetrations were made. The sailplane at this time ($\sim$1601 MDT) is approximately over the Butler airstrip [Grover coordinates (2,21)] at an altitude of 3.6 km, and the direction of the photo is south-southeast.

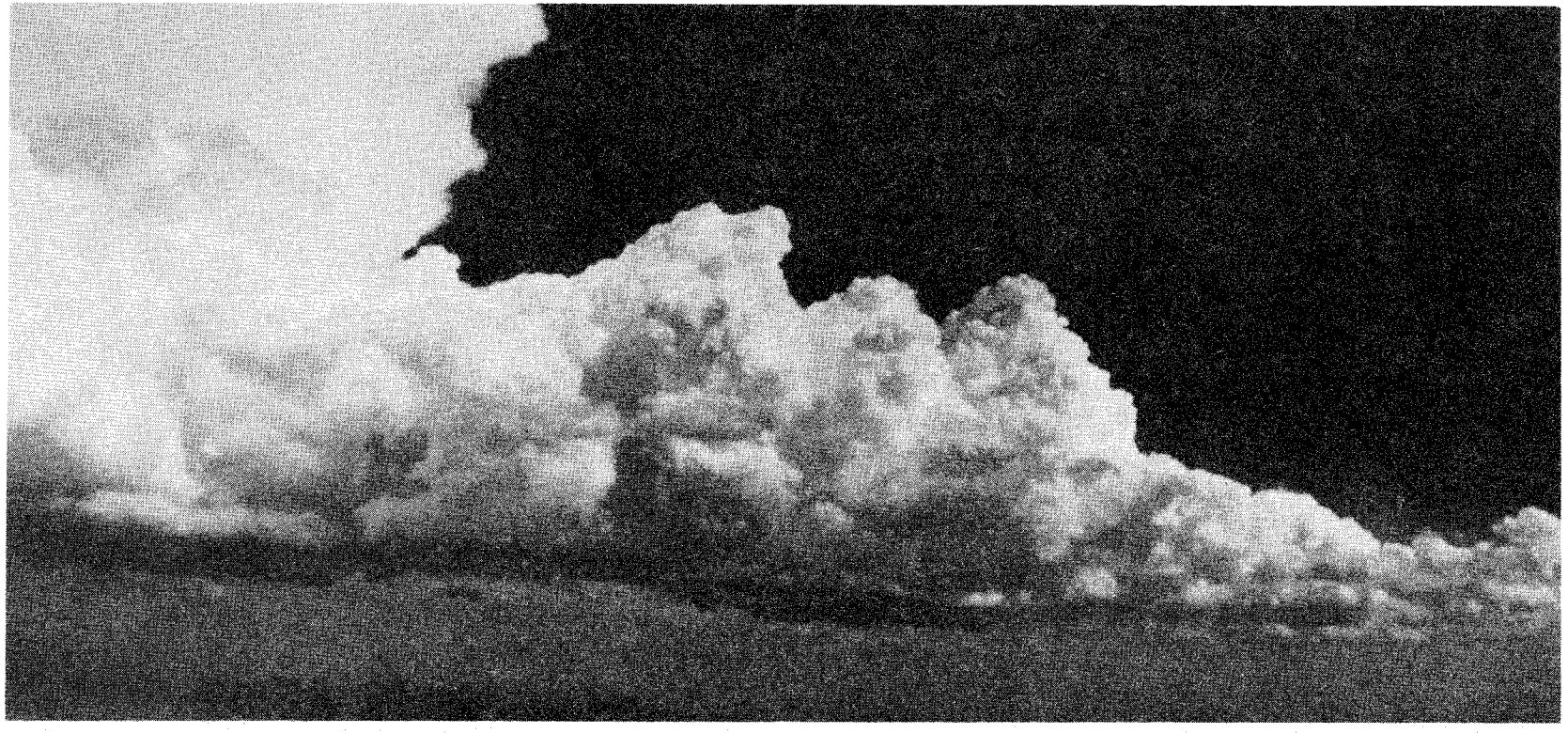

Fig. 12. Photograph of the developing southwest flank of the storm complex where the sailplane penetrations were made. Time is ~1601 and direction viewed is south-southeast.

IV. OTHER DATA

A. MESONETWORK

Data obtained from all stations have been reduced and are plotted on microfilm from 1400 to 2000, with the exception of the PAM stations which shut down after 1725 due to a power failure. The entire network is plotted on a gridded map in 5 min intervals with values for T, T_d, pressure, θ, θ_e, and mixing ratio as well as the winds.

B. DOPPLER

There is a good possibility that dual-Doppler coverage existed for the 1525 and 1530 scans from NOAA-D and CP-4. The resolution of CP-4 degraded after this, but the 1540 scan of NOAA-D should be usable. None of these data have been processed or edited during these scan periods.

C. TIME-LAPSE PHOTOGRAPHY

Grover, Lindbergh and Greeley cameras were all obscured from the southwest flank during the time of the sailplane penetrations.

D. STILL PHOTOGRAPHS

Some photographs from the sailplane show the first echo study area (see Fig. 12), and two panoramic sweeps of the west side of the general storm mass were photographed between 1600 - 1605. Photogrammetric analysis is questionable due to no sailplane position or camera angle data.

Other work related to this day and the first echo case are the mature storms case study (Fankhauser, 1978; Harris *et al.*, 1978; Knight

et al., 1978), a paper on moist adiabatic ascent in northeast Colorado (Heymsfield *et al.*, 1978), and papers involving precipitation analysis (Dye and Martner, 1978; Long 1978). The large multicellular complex which evolved from the line of discrete echo systems described in the radar history section is the focus of the mature storms case study. The echo system or storm element investigated by the sailplane and 10UW was comparable to many similar developments that dominated the evolution of the larger storm complex. Quantitative comparisons of updraft strength and dimension between the first echo case and the mature storms case are not possible due to the airspeed recovery problem on 10UW mentioned earlier. However, there is qualitative agreement between the two cases of an updraft-echo development relationship that is described in detail in the mature storms case study papers. Continuing work of the mature storm study on this day will involve extensive radar (with multiple-Doppler wind fields), aircraft (including T-28 penetrations), hailstone, and conventional surface and upper air data.

V. SUMMARY

The sailplane penetrated a growing turret on the west side of a developing storm cell prior to the time of the radar "first echo" at the sailplane's altitude. The storm cell was located on the southwest flank of a major storm complex, the same area where many earlier storm cells had formed and subsequently moved northward through the general storm mass. The sailplane made two and a half sprials in the same location during the 7 min in-cloud period, encountering strong updrafts (maximum, 22 m sec^{-1}) and increasing ice particle concentrations with time. Radar support was insufficient in providing a total reflectivity history about the sailplane, although it appears that the flight was timed and positioned correctly to encounter first echo conditions. The maximum reflectivity encountered was $\sim$15 dBZ_e, and precipitation-sized particles were exclusively ice. No liquid drops greater than cloud droplet size were detected.

The second penetration period of 1536-1550 was in scattered conditions north of the earlier penetration, and yielded little interesting data.

The Wyoming Queen Air 10UW made seven cloud penetrations between 1520 and 1555 in the developing southwest flank. The penetrations were made at altitudes between 5.0 and 5.5 km with the first three directly underneath the sailplane and the subsequent four in the same area with respect to the radar structure. Temporal continuity of updrafts along the western edge were detected, with graupel generally present in reflectivities > -5 dBZ_e. Ice particles appeared to be present in

updraft regions in Passes V, W and A. Further examination of these data may yield information on particle growth to precipitation size, although the lack of Doppler radar data and the complexity of the cellular structure makes air motion and particle trajectory analyses speculative.

APPENDIX A

GROVER RADAR SPECIFICATIONS

The radar reflectivity data presented in the text were obtained by the Grover S-band radar (CP-2) during the 1976 field season. The specifications of the radar set are given in the table below.

Table 1. Grover S-band Radar Specifications

Antenna	
Horizontal beamwidth (deg.)	0.99
Vertical beamwidth (deg.)	0.94
Gain (dB)	44.2
Transmitter	
Frequency (MHz)	2801
Wavelength (cm)	10.7
Peak power (kw)	650
(dBm)	88.1
PRF (s^{-1})	937.5
Pulse duration (μs)	0.92
Receiver (logarithmic)	
Minimum detectable signal (dBm)	-107.4

In calculating Z_e (effective reflectivity) from the radar equation for meteorological targets, $|K|^2$ was set equal to 0.93, which is the value for water targets. ($|K|^2$ is related to the complex index of refraction of the target.) The CP-2 radar has an unambiguous range of 105 km.

Methods used for calibration of the radar and more detailed information about the radar are described in Foote *et al.* (1976) and Eccles (1975).

APPENDIX B

SAILPLANE INSTRUMENTATION

The meteorological parameters of interest measured or calculated from measurements by the NCAR/NOAA sailplane are pressure altitude, vertical airspeed, temperature, liquid water content, cloud droplet spectrum and precipitation particle concentration and type. Data are sampled every second and recorded on magnetic tape at a ground station via FM telemetry from the sailplane. True airspeed is generally about 40 m sec^{-1} and bank angle in the spiral flight mode is roughly 15 to 30°.

Pressure Altitude

A Hamilton Standard pressure transducer is used to measure pressure, which is then reduced to altitude using a nearby sounding. Accuracy is about ±10 m. The resolution, which is important in the calculation of vertical airspeed, is 0.5 m. Electronic noise occasionally interrupts a timing circuit directly involved in the measure of pressure. When this happens, the altitude always deviates to lower values, and these temporary drops are quite apparent on the altitude plot of the sailplane data.

A variometer is also used to determine pressure altitude by summing rates of change with time and adding the resultant height to the initial altitude of the sailplane. Although the response time of this instrument is slower than that of the Hamilton Standard device, agreement between the two is usually very good. Errors, brought about by

sharp gradients of updrafts or downdrafts or other flight phenomena that are not adequately measured by the variometer, are cumulative, with the result that the altitude measured in this way can drift to 500 m in 10 min.

Vertical Airspeed

The equation for calculating vertical airspeed (see Dye and Toutenhoofd, 1973) is:

$$w = \frac{dz}{dt} + \frac{|\vec{v}|D}{mg} + \frac{1}{2g}\frac{d}{dt}\left(|\vec{v}|^2\right) \quad ,$$

where w is the vertical airspeed, t the time, $\vec{v}$ the sailplane velocity, D the drag force on the sailplane, m the mass of the sailplane and g the acceleration due to gravity. Assumptions include hydrostatic equilibrium of the atmosphere, no side slip of the sailplane and no abrupt flight maneuvers. Also, vertical speed induced by horizontal wind changes is ignored. In other words, it is assumed that the horizontal wind is steady, or that over a few seconds, small-scale fluctuations average out to zero. Uncertainty from this calculation when the sailplane is spiralling in clouds is about 2 m sec^{-1}. The most important variables are rate of change of altitude and true airspeed. Minor variables are temperature, pressure, bank angle, angle of attack, and indicated airspeed which are used to derive the true airspeed and the sailplane's drag force. Significant errors in vertical airspeed are caused by errors in the major input parameters. True airspeed can be lost altogether due to icing of the pitot tube, or false altitude changes can be caused by the deviations in the Hamilton Standard derived

altitude mentioned above. Vertical airspeed can be calculated using the Hamilton Standard derived $\frac{dz}{dt}$ or using the dz/dt determined directly by the variometer. Usually the vertical airspeed plots derived by the two methods are nearly identical.

Temperature

Air temperature is measured by a reverse flow temperature probe, designed for the slow flight speeds of the sailplane. Discussion of the calibration and intercomparison of this probe with other sources is presented in Heymsfield *et al.* (1978). Wetting of the sensing diode when in cloud does not appear to occur with the sailplane probe, and the stated accuracy of ±0.5°C appears to be correct. Another source of air temperature data is collected by a "window" probe, and is usually plotted with the reverse flow temperature. The "window" probe is an identical sensing diode exposed to the airstream in a vent located in the nose of the sailplane. The accuracy of the diode is also ±0.5°C but it inherently becomes wetted or iced during cloud penetrations.

There is one significant problem with the temperature data. When the communications radio is transmitting, RF noise influences the voltage drop across the diode, thereby causing increased temperature readings. This noise is evident in other (minor) data channels as well as in the sharp changes in the temperature plot, and is easily identified. It has not been edited out of the data plots presented in the text.

Liquid Water Content

A Johnson-Williams hot-wire device is used for measuring liquid water content (LWC). Calibration and comparison discussions are presented in Heymsfield *et al.* (1978). Best estimates suggest an accuracy within ±20%. However, when the sailplane encounters high liquid water contents in supercooled conditions for extended periods, the probe's strut accumulates enough ice apparently to interfere with the flow to the sensor. This is usually identifiable by the "spikey" appearance of the J-W LWC trace, which has also become uncorrelated with the vertical airspeed trace. This condition occurs only when the high liquid water conditions have existed for roughly 10-15 minutes.

The FSSP (described below) integrated cloud droplet spectrum also provides a measure of LWC, and is plotted with the J-W output.

Cloud Droplet Spectrum

A Particle Measuring Systems (PMS) forward scattering spectrometer probe (FSSP), mounted on the sailplane, measures cloud droplet spectra. This probe, reported in various articles (for example see Knollenberg, 1976), sizes particles 2-30 μm in diameter with a suggested error of ±10% or ±2 μm, whichever is greater. Concentration accuracy had not been determined, and comparison with the J-W LWC, vertical airspeed, and different flight conditions suggested that the FSSP on the sailplane was measuring concentrations lower than would be expected.

Investigation of the probe's electronic design by personnel at the University of Wyoming revealed that coincidence errors, coupled with a retriggerable electronic delay (which allows time for the electronics to

size and count pulses), results in a greatly reduced measured droplet concentration in comparison to the true concentration. Assuming that the time between individual droplets can be described by a Poisson distribution, Dr. W. A. Cooper of the University of Wyoming has shown that the equation,

$$N_m = N_o \exp\left(-uA\tau N_o\right) ,$$

can be used to determine the measured concentration (N_m) from the true concentration (N_o), where u is the true airspeed, A the total sampling area, and τ the delay time. For the sailplane FSSP and the range of droplet concentrations found in northeastern Colorado, N_m is a monotonic function of N_o. However, for the University of Wyoming's Queen Air N10UW, N_m is bi-valued with the maximum at $\sim$500 droplets cm^{-3}. For the South Dakota School of Mines and Technology's armored T-28, the plateau value is about 200 cm^{-3} measured concentration.

The FSSP data presented in the text have not been corrected for this error.

Ice particles passing through the sample area apparently give multiple, specular reflections which are measured by the FSSP as individual particles. In regions where considerable ice particles are present, this artifact is most noticeable as a spectrum tail in the larger channels and invalidates any measurements in the largest 7 or 8 channels as well as the calculated droplet dispersion. The counts in these regions should not be used as a measure of the ice particle concentration, since one ice particle apparently gives rise to more than one apparent droplet count.

An added problem with the FSSP data arises due to icing of the probe. After only a few minutes of in-cloud sampling, icing of the FSSP causes noticeable degradation of the data. Wind tunnel tests suggest that icing primarily causes a shift of the spectrum to smaller sizes, but examination of field data also shows a definite decrease of concentration with time. Apparently, the erroneous measurements are caused by wetting or icing of the prism and mirror, and also by the accumulation of ice on the front of the sampling tube. No attempt has been made to correct the data for these problems, due to the variable results found in the wind tunnel tests. Therefore, even when the concentrations have been corrected for coincidence errors, the FSSP data are definitely not trustworthy beyond a few minutes into a cloud penetration, and the reliability might be questionable even in the first few minutes.

Cloud Particle Camera (CPC)

Cloud particle concentrations, sizes and types are measured by the Cannon cloud particle camera which photographs atmospheric particles *in situ* (Cannon, 1974). The size range measured by the sailplane CPC is 16 μm to 48 mm diameter, and the sampling volume increases with the particle size. For photographic images $\geq$ 170 μm diameter, water droplets can be distinguished from ice particles by the two-dot method (i.e., refracted images from the two flashlamps by the water drop). The camera has a film capacity of 3200 frames, which is equal to 27 minutes of exposure time at the maximum rate of 2 frames per second.

About the only flight-related difficulty encountered with the CPC occurs when the airspeed is incorrect. This affects the synchronization

of the rotating mirror with the speed of the sailplane, which is necessary to allow stop-action photography of the particles passing through the sampling volume. An incorrect airspeed will blur the images on the film, while the loss of airspeed, as may be caused by icing of the pitot tube, will cause blank frames on the film since the rotating mirror and the flashlamps will have ceased to operate. This problem is easily detected in examination of the film along with the true airspeed data trace.

APPENDIX C

WYOMING QUEEN AIR 10UW INSTRUMENTATION

The following table is the complete set of instruments flown on 10UW during the 1976 field season, and has been provided by the Department of Atmospheric Sciences, University of Wyoming. Data from all of these instruments have not been presented in this Note.

UNIVERSITY OF WYOMING RESEARCH AIRCRAFT INSTRUMENTATION

Part 1: Continuous Variables

Parameter Measured	Instrument Type	Manufacturer and Model Number	Combined Performance of Transducer, Signal Conditioning and Conversion			
			Range	Accuracy	Time Constant	Useable Resolution*
Time	Crystal osc	University of Wyoming, Dept. of Atmos. Science	12 mo	1 sec	NA	1 sec
Temperature	Platinum resistance	Rosemount Eng. Co. 510BF9 Bridge Model 102 Probe	±50°C	0.5°C	1 sec	0.1°C
Temperature	Platinum resistance, reverse flow	NCAR - probe Minco Inc. - element	±50°C	0.5°C	1 sec	0.1°C
Dew Point	Peltier cooled mirror	Cambridge System Inc. Model 137-C3	±50°C	1°C	5-10 sec	0.3°C
Liquid Water	Hot wire	Bacharach Inst. Co., Model LWH	0-3 gm/m^3	0.3 gm/m^3	1 sec	0.1 gm/m^3
Turbulence	Pressure	Meteorology Research Inc. Model 1120	0-10 IT	1 IT	3 sec	0.1 IT
Radiation (upper)	Pyranometer	Eppley	0-1.77 cal cm^{-2} min^{-1}		1 sec	
Radiation (lower)	Pyranometer	Eppley	0-1.654 cal cm^{-2} min^{-1}		1 sec	
Altitude	Total pressure	Rosemount Eng. Co. Model 1301 A 2A A4AX	0-15 psia	0.015 psia	1 sec	0.007 psia

*See footnote next page.

UNIVERSITY OF WYOMING RESEARCH AIRCRAFT INSTRUMENTATION

Part 1: Continuous Variables (contd.)

Parameter Measured	Instrument Type	Manufacturer and Model Number	Combined Performance of Transducer, Signal Conditioning and Conversion			
			Range	Accuracy	Time Constant	Useable Resolution*
Indicated Airspeed	Differential pressure	Rosemount Eng. Co. Model 1301 B 1A D1AX	0-3 psid	0.003 psid	1 sec	0.002 psid
Aircraft Manifold Pressure	Pressure	Rosemount Eng. Co. Model 1331	0-50 psia	0.1 psia	1 sec	0.1 psid
Rate of Climb	Calibrated leak pressure	Ball Eng. Co.	±3000 fpm	50 fpm	1 sec	50 fpm
Heading	Magnetic	King Radio Corp. Model KPI 550A	0-360°	±1°	1 sec	10
Position (azimuth)	VOR	King Radio Corp. Model KNR 660	0-360°	±1°	1 sec	10
Position (distance)	DME (VOR)	King Radio Corp. Model KDM 700	0-100 n mi	0.1 n mi	1 sec	0.1 n mi
Ground Speed	Doppler radar	Singer-Keorfott Model APN-153V	80-800 kt	1 kt	1 sec	1 kt
Drift Angle	Doppler radar	Singer-Keorfott Model APN-153V	±30°	0.35°	≈5 sec	0.35°
Yaw	Vane-driven synchro	University of Wyoming, Dept. of Atmos. Science	±180°	0.5°	1 sec	0.35°

*Values quoted are estimates of overall useable resolution which can be expected for actual flight conditions. Theoretical resolutions are one part in 4095 for all the above parameters except for heading, position, ground speed, drift angle and yaw, which are one part in 1023.

UNIVERSITY OF WYOMING RESEARCH AIRCRAFT INSTRUMENTATION

Part 2: Discrete Variables

Parameter Measured	Instrument Type	Manufacturer and Model Number	Range	Resolution	Sampling Rate	Useable Concentration
Cloud Droplets	Optical scattering	Particle Measuring Systems Model ASSP	0.5-7.5μm dia 1-15μm dia 2-30μm dia 3-45μ	(15 channels)	850 cm^3 km^{-1}	1-10^3 cm^{-3}
Cloud Droplets	Slide replicas	University of Wyoming, Dept. of Atmos. Science	4μm dia and up	15%	25 cm /slide ∿1 slide/min max	
Ice Crystals	Shadow imaging	Particle Measuring Systems Model 2-D	25μm dia and up	25μm	50 ℓ km^{-1}	10^{-2}-10^5 ℓ^{-1}
Ice Crystals	Direct sampling in decelerator; microscope examination	University of Wyoming, Dept. of Atmos. Science	10μm dia and up	2μm	50 ℓ km^{-1}	10^{-2}-10^5 ℓ^{-1}
Aerosols	Optical scattering	Particle Measuring Systems Model ASAS	0.08-0.21μm dia 0.18-0.43μm dia 0.30-0.69μm dia 0.45-3.90μm dia	(15 channels)	0.18 cm^3 sec^{-1}	1-10^3 cm^{-3}
Aitken Nuclei	Expansion chamber	Environment One, Inc., Model Rich 100	50Å and up	NA	50 cm^3 sec^{-1}	300-10^7 cm^{-3}

Aerosol Collector: Filter sampler: sets of four filters, max 45 mm dia, total flow rate 60 ℓ min^{-1}

Air Sampler: Bag samples: 120 ℓ filled over 1 min

Precip Collector: Bottle sampler held outside aircraft

Precip Impactor: Foil with gridded backing held outside aircraft

Events: Ten selectable events marked from each of three stations

REFERENCES

Cannon, T. W., 1974: A camera for photography of atmospheric particles from aircraft. *Rev. Sci. Instru. 45*, 1448-1455.

Dye, J. E., and B. E. Martner, 1978: The relationship between radar reflectivity factor and hail at the ground for northeast Colorado thunderstorms. *J. Appl. Meteor. 35*, in press.

_____, and V. Toutenhoofd, 1973: Measurements of the vertical velocity of air inside cumulus congestus clouds. *Preprints Eighth Conf. on Severe Local Storms*, Denver, Amer. Meteor. Soc., 33-34.

Eccles, P. J., 1975: Developments in radar meteorology in the National Hail Research Experiment to 1973. *Atmos. Tech. Winter 1974-75*, NCAR, 34-45.

Fankhauser, J. C., 1978: A complex multicellular hail and rainstorm, Part I. Large scale influences, mesoscale features, and general storm structure. To be published as an NCAR Technical Note.

Foote, G. B., R. C. Srivastava, J. C. Fankhauser, F. I. Harris, T. J. Kelly, R. E. Rinehart, C. G. Wade, P. J. Eccles, E. T. Garvey, M. E. Solak, R. E. Vaughan, B. E. Weiss and R. J. Wolski, 1976: Final Report - National Hail Research Experiment 1972-1974. Volume IV: Radar Summary. NCAR, 326 pp.

Harris, F. I., J. C. Fankhauser and J. R. Miller, 1978: A complex convective storm system studied by multiple-Doppler radar analysis. *Preprints Eighteenth Conf. on Radar Meteor.*, Atlanta, Amer. Meteor. Soc., 252-259.

Heymsfield, A. J., P. N. Johnson and J. E. Dye, 1978: Observations of moist adiabatic ascent in northeast Colorado cumulus congestus clouds. *J. Atmos. Sci. 35*, in press.

Knight, C. A., F. I. Harris, J. C. Fankhauser and N. C. Knight, 1978: Precipitation development in a severe, continental, multicell hail and rainstorm. *Preprints Conf. on Cloud Physics and Atmos. Electricity*, Issaquah, Amer. Meteor. Soc., 514-521.

Knollenberg, R. G., 1976: Three new instruments for cloud physics measurements: the 2-D spectrometer, the forward scattering spectrometer probe, and the active scattering aerosol spectrometer. *Preprints Int. Conf. on Cloud Physics*, Boulder, Amer. Meteor. Soc., 554-561.

Long, A. B., 1978: Design of hail measurement networks. *Atmosphere-Ocean 16*, 35-48.